ISAS - INTERNATIONAL SCHOOL FOR ADVANCED STUDIES

Phonon Softening and High-Pressure Low-Symmetry Phases of Cesium Halides from First-Principles Techniques

Thesis submitted for the degree of

"Doctor Philosophiæ"

CANDIDATE

Marco Buongiorno Nardelli

SUPERVISOR

Prof. Stefano Baroni

October 1993

TRIESTE

SISSA - SCUOLA INTERNAZIONALE SUPERIORE DI STUDI AVANZATI

TRIESTE

Strada Costiera 11

SISSA ISAS
SCUOLA INTERNAZIONALE SUPERIORE DI STUDI AVANZATI
INTERNATIONAL SCHOOL FOR ADVANCED STUDIES

Phonon Softening and High-Pressure Low-Symmetry Phases of Cesium Halides from First-Principles Techniques

Thesis submitted for the degree of

"Doctor Philosophiæ"

CANDIDATE

Marco Buongiorno Nardelli

SUPERVISOR

Prof. Stefano Baroni

October 1993

Table of Contents

1 Introduction

The properties of condensed matter at ultrahigh pressures are of considerable current interest not only in solid state physics, but also in geophysics and in material science. From a fundamental point of view, the behaviour of matter under extreme pressure conditions shed light on the properties of bonding through the study of the modification of the electronic structure induced by the decrease of the interatomic distances. These modifications can lead the system to new ground states with different physical and chemical properties, thus providing the driving mechanism of structural phase transitions.

The pressures that are attained in modern high-pressure experiments range up to a few thousands of GPa. The typical pressure of the inner mantle of earth (from -600 to -2890 Km where $P \approx 170$GPa), falls in this range. Therefore these studies are of considerable interest for geophysics. Changes in the structure of constituents of the mantle, creating discontinuities in the density, are in fact crucial in the study of the dynamics of earthquakes. Moreover, understanding the mechanical properties of matter in extreme pressure and temperature conditions is of paramount technological importance in order to improve the production and synthesis of new materials.

High-pressure experiments have expanded continually during this century. In recent

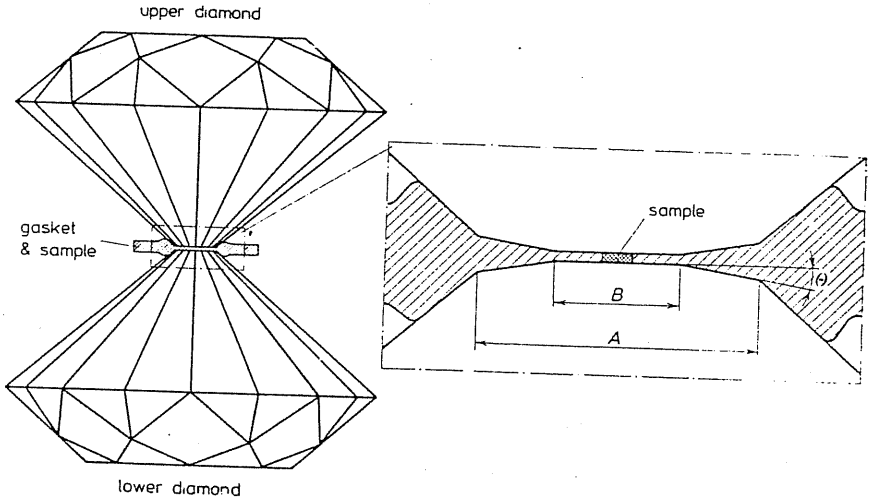

Figure 1.1: Schematic diagram of the high-pressure cell with diamond anvil, according to Mao and Bell [1]. Distance from top surface of upper diamond to bottom surface of lower diamond is about 5mm. The sample is 250μm.

years, the diamond anvil cell technology has opened a major breakthrough in the physics of materials at very high pressures, increasing the range of attainable pressures, and allowing to achieve a more homogeneous and hydrostatic pressure environment. This improvement has made precise physical measurements possible under a wide range of pressures, and has determined a renewed interest in this field, permitting fruitful comparisons between theory and experiments. Hydrostatic pressures are in general obtained by placing a sample in a transmitting medium which is acted upon by outside pressure. In Fig. 1.1 a schematic diagram of a high-pressure cell with diamond anvil is drawn.

One of the most unexpected features of solids at high pressure is the spontaneous symmetry lowering of some cubic compounds, such as alkali halides. Alkali halides exhibit a large variety of behaviours at high pressure. Those compounds that crystallize in the cubic-B1 structure (like NaCl and KCl) undergo a phase transition to the cubic-B2 (CsCl-like) structure in a pressure range of few GPa. This structure is observed to be stable

up to very high pressure (100 GPa) for compounds like NaCl and KCl [2]. Cesium salts, that crystallize in the cubic-B2 structure, display a distortion of the cubic cell at pressures corresponding to a residual volume $V/V_0 \approx 0.5$. These materials are the subject of the present study.

Since the pioneering work of Madelung and Ewald [3], alkali halides have been the subject of much experimental and theoretical work. They are the simplest and most typical ionic solids, and even though innumerable studies have been devoted to them, still today they remain subject of investigation particularly since the introduction of the diamond anvil cells which has opened the access to previously unaccessible portions of their phase diagram. Thanks to these new techniques, new and unexpected phases have been discovered, and the modifications of the electronic properties related to bond-overlap metallization have been studied. Among these compounds, CsI has been the subject of intense interest. It is the softest among alkali halides and it has the smallest band gap. For these reasons it is an ideal candidate to evidence an insulator to metal transition upon increasing pressure. Looking for the band-overlap metallization of this compound, new and unexpected phases stabilized by the large applied pressure have been discovered. Experimentally, the insulator-to-metal transition has been found by Reichlin *et al.* [10] from infrared reflectivity measurements at an estimated pressure of 1.1 ± 0.1 Mbar. As it is evidenced in Fig. 1.2, a general consensus on this estimate does not exist yet [11].

The first systematic studies on the low-symmetry phases of Cesium halides under high pressure date back to 1984. From energy-dispersive X-ray diffraction experiments Huang *et al.* [4] and Knittle *et al.* [5] were able to observe that all the cubic-B2 Cesium halides, CsI, CsBr, and CsCl, undergo a transition which lowers the cubic symmetry of the system at a

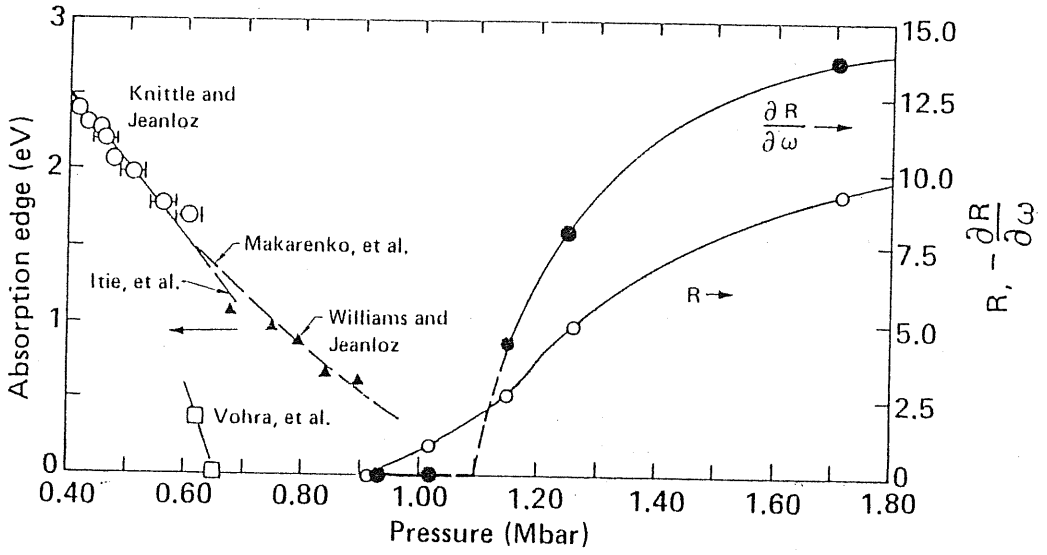

Figure 1.2: Summary of high pressure optical properties of CsI from Ref. [10]. Together with the reflectivity data of Reichlin et al., other measurements by other groups are shown. For reference see Reichlis's original paper.

pressure corresponding to a molar volume $v^* = V/V_0 \approx 0.54$ where V_0 is the equilibrium volume. The observed transition pressures are of 39, 53, and 65 GPa for CsI, CsBr and CsCl respectively [5]. This symmetry lowering manifests itself through the splitting of the (110) diffraction line into two peaks which are interpreted as corresponding to the (101) and (110) unequivalent reciprocal lattice vectors of a tetragonal structure (see Fig. 1.3). Correspondingly, the (211) peak splits into the (112) and (211) of the tetragonal phase. In their measurements both the authors observed no detectable discontinuity in any physical observable, and therefore they classified the phase transition as second order. However, general group-theoretical considerations indicate that this cannot be so. In fact, it is a general and well established result that a transition from a cubic to a tetragonal phase in which the only order parameter is the unit cell shape, *i.e.* the strain, cannot be second order [6]. However, as the transition is nearly continuous within experimental accuracy,

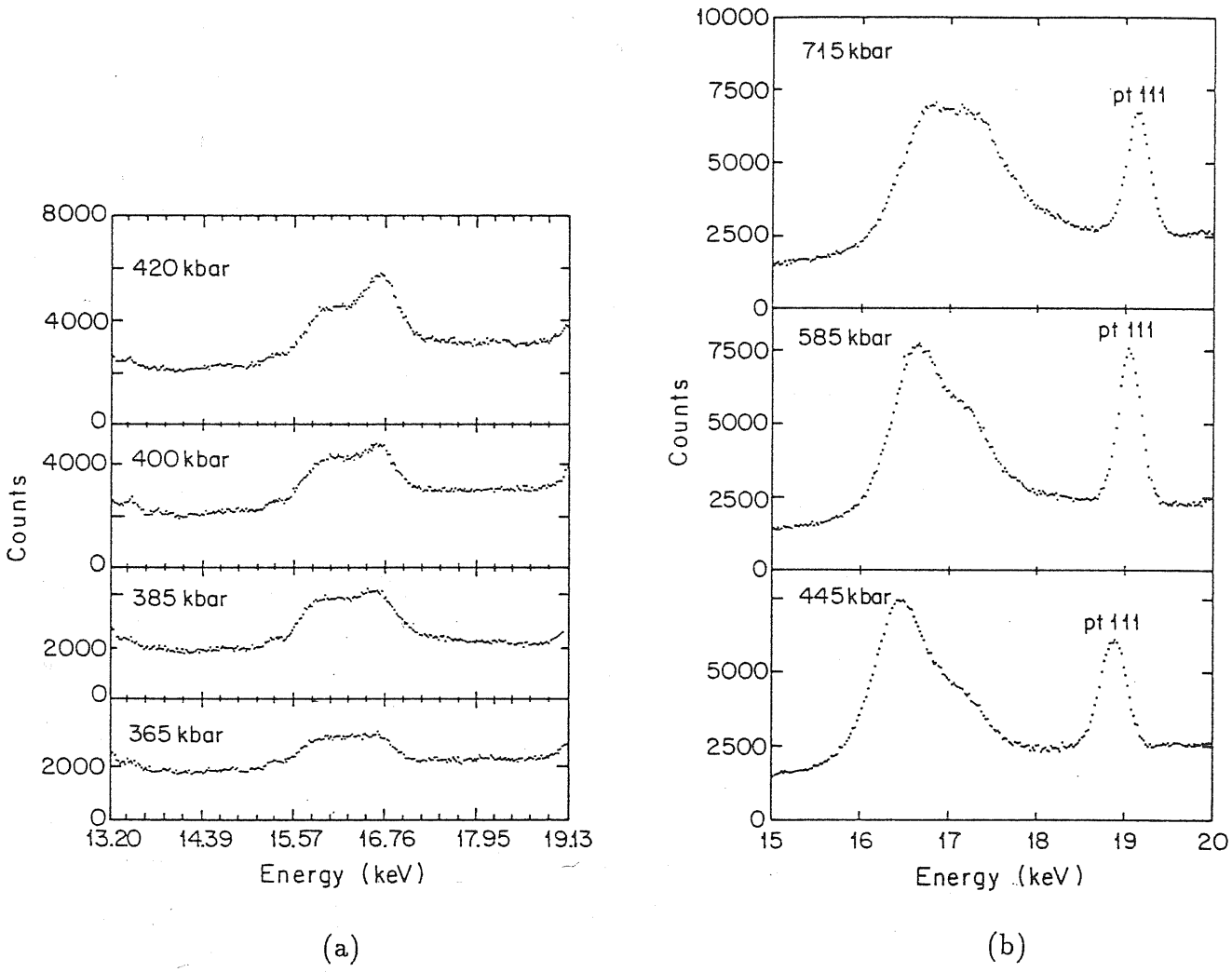

Figure 1.3: Curves showing the sequential splitting of the 110 peaks in CsI (a) and CsBr (b). From Ref. [4].

we conclude that its first order character is very weak. Even though the measurements of the two groups suffered of a rather limited experimental resolution and of a not perfectly homogeneous and hydrostatic pressure, the results and the emerging picture are consistent with each other, apart from minor quantitative discrepancies in the measurement of the transition pressures.

In another experiment, Asaumi [7] reported on a successive transition in CsI from the tetragonal to a simple orthorhombic structure (space group D^1_{2h}) at a pressure of 56 GPa.

Such a transition however has not been observed by others, nor it was predicted in any theoretical calculations. Due to the limited resolution of the spectra and to the difficulty in obtaining real homogeneous and hydrostatic pressure no final conclusions can be drawn on the basis of this set of data only.

The first theoretical study of the cubic-to-tetragonal transition has been performed by Vohra *et al.* [8]. Using a Born-Meyer potential to model the interionic interactions, they were able to explain the transition in terms of the competition between electrostatic and repulsive interactions, confirming the first-order character of the transition. They pointed out that the tetragonal distortion is due to the macroscopic instability of the CsCl lattice which is related by the vanishing of the shear constant $c_s = \frac{1}{2}(c_{11} - c_{12})$ (in cubic compounds c_s is the appropriate elastic constant for tetragonal distortions). They also investigated the possibility of observing a further distortions of the lattice from tetragonal to orthorhombic, but the minimum of the lattice energy was always found at $b/a = 1$, at all pressures, and no orthorhombic phase was predicted.

Some investigations on CsI have been carried out also from first principles. Christensen *et al.* [9] studied the transition in the framework of Linear Muffin Tin Orbital in the Atomic Sphere Approximation, in connection to the metallization. They globally confirmed the picture already proposed by Vohra *et al.*, and they were able to predict from first principles the cubic-to-tetragonal transition and to describe the modifications in the electronic structure induced by pressure. In particular, they predicted metallization of CsI to occur at $V/V_0 \approx 0.50$ corresponding to a pressure of about 0.65 Mbar. Baroni and Giannozzi [12] performed an ab-initio pseudopotential study of the transition. Also in this framework the cubic-to-tetragonal first-order transition has been confirmed, as it is clear in Fig. 1.4,

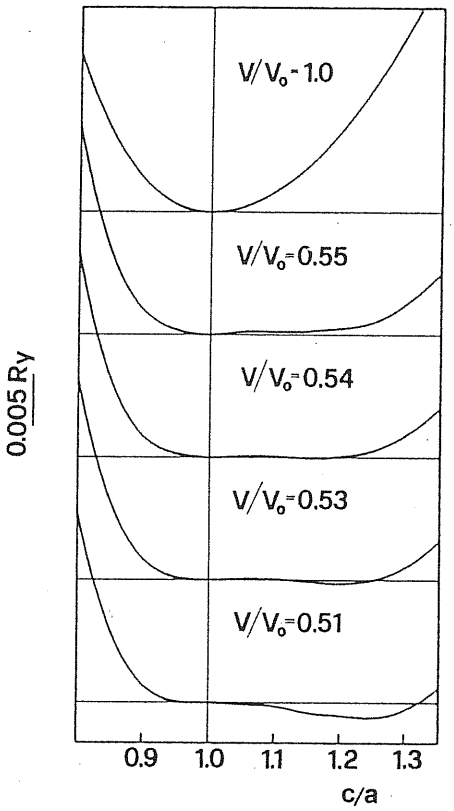

Figure 1.4: Crystal energy per cell of CsI as a function of c/a for various volumes of the unit cell, referred to the calculated zero pressure volume V_0. From Ref. [12].

where the crystal energy is plotted as a function of the c/a parameter of the tetragonal cell for various residual volumes V/V_0.

In 1989, new and unexpected features emerged from the X-ray diffraction experiments performed by Mao *et al.* [13] on CsI. Using a more sophisticated experimental set-up and a synchrotron radiation source, they were able to identify a continuous distortion of the CsI cell from the cubic B2 to a hexagonal-closed-packed (HCP) structure passing through an intermediate orthorhombic structure. In Fig. 1.6 we display the X-ray diffraction pattern of CsI taken at 77.5 GPa in the energy range close to the (110) diffraction peak of the undistorted cubic structure. It is observed that the (110) peak splits into three

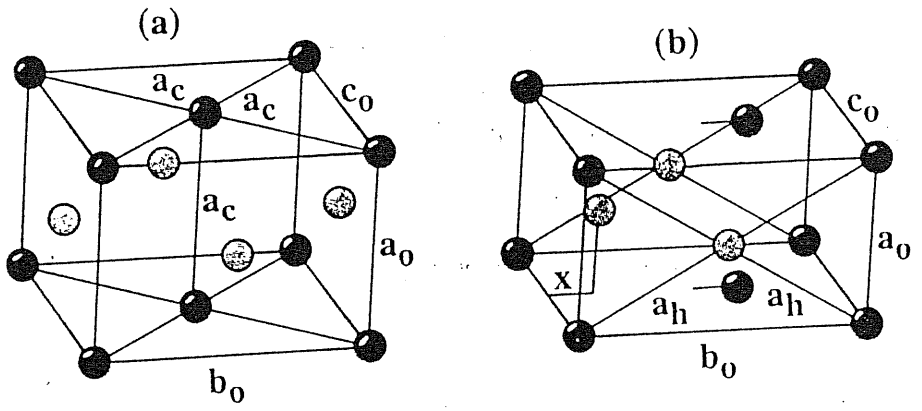

Figure 1.5: Structure drawings indicating the nature of the phase transition in CsI. (a) The original cubic B2 cell; (b) the orthorhombic structure with the gliding of the cubic (110) plane. Solid spheres, Cs; empty spheres, I. The subscripts o, c, and h denote the lattice parameter of the different structures. From Ref. [13].

components, whereas two additional lines appear on the low- and high-energy sides of the triplet, corresponding to two diffraction peaks which are forbidden in the B2 structure. This diffraction pattern can be explained by assuming an orthorhombic distortion of the cubic cell, as depicted in Fig. 1.5. In the undistorted B2 structure the unit cell is characterized by $a_o = a_c$, $b_o = c_o = \sqrt{2}a_c$,, as indicated in Fig. 1.5(a). The orthorhombic cell is characterized by a departure of the three lattice constants from the above ideal values and by a gliding of the cubic (110) plane, as indicated in Fig. 1.5(b). In the absence of this gliding there would exist a smaller unit cell describing the same structure and the peaks corresponding to the cubic $(\frac{1}{2},\frac{1}{2},1)$ and $(\frac{3}{2},\frac{1}{2},0)$ would be forbidden. The observation of diffraction lines corresponding to these two vectors is indeed a direct manifestation of the postulated gliding whose magnitude is measured by the parameter x indicated in Fig. 1.5(b). In the final HCP structure one has $a_o = a_h$, $b_o = \sqrt{3}a_h$, $c_o = c_h$, ($c_h/a_h = 1.633$ for ideal close packing), and $x = b/6$. Even though the intermediate structure has an orthorhombic symmetry, it is geometrically different from the previous assignment [7], and the space group of the postulated structure is C^1_{2v}.

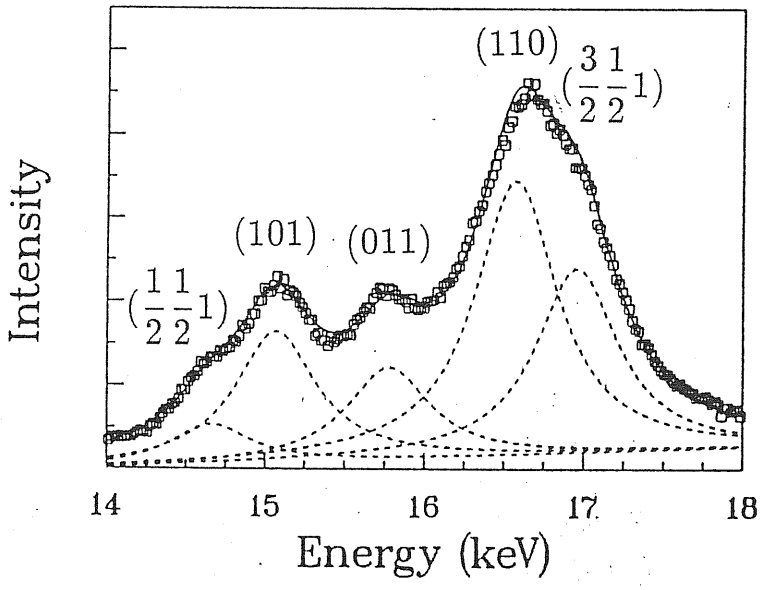

Figure 1.6: Energy-dispersive x-ray-diffraction pattern of CsI at 77.5 Gpa showing deconvolution of the quintuplet. From Ref. [13].

The observed splitting and peak intensities evolve continuously from 15 to 100 GPa, showing a single orthorhombic phase with variable parameters; even though the experiments seem to indicate a continuous distortion from the cubic to the orthorhombic structure, a weak first-order character of the transition cannot be ruled out. The starting point of the phase transition, characterized by the splitting and broadening of the B2 diffraction lines, is observed at pressures as low as 15 GPa. However, below 45 GPa the splitting is not large enough to allow an unequivocal identification of the orthorhombic structure.

Nearly at the same time of the experiments by the Mao's group, other data were published by a russian team [14]. From the analysis of these measurements they framed the conjecture that the cubic phase of CsI transforms directly into an orthorhombic one, thus confirming the measurements of Mao *et al.* However, because of a poorer resolution

in the recorded spectra, they were not able to clearly assign the symmetry of the new phase and to identify any displacement of atoms in the cell.

As this short review has shown, the theoretical and experimental information on structural phase transition in Cesium halides and particularly in CsI are somehow confused. A clear assignment of the high-pressure phases is in general difficult, because of the discrepancies between theoretical results and the new experimental measurements and between experimental data themselves. Moreover also the character and the intimate mechanism of the transition have not been explained. The purpose of this thesis is to shed light on the characteristics of the low-symmetry phases of Cesium halides and on the mechanisms which determine the structural transition under pressure, and to provide a general classification of the high-pressure structures of a larger number of alkali halides.

The gliding of the (110) plane described by Mao *et al.* represents a lattice distortion very similar to a zone-border acoustic phonon propagating with a wavevector $\mathbf{q} = \frac{\pi}{a}(110)$ and polarized along $(1\bar{1}0)$. The fact that this lattice distortion is energetically favoured suggests that the above mentioned phonon mode softens upon an applied pressure. This softening is intimately related to the previously postulated cubic-to-tetragonal transition which is associated to a dramatic softening of the shear constant, that is in fact proportional to the square of one of the two transverse sound velocities along (110). These considerations suggest that a coherent picture of the low-symmetry phases of these compounds may be obtained within a Landau theory of phase transitions (LTPT), in which the amplitude of the above zone-border phonon plays the role of an order parameter.

In this thesis we present a complete study of the structural and lattice-dynamical properties of Cesium halides based on modern techniques for calculating electronic

and vibrational properties of crystals. Our calculations are based on density functional theory (DFT) and density functional perturbation theory (DFPT). Our results have been rationalized using LTPT which has allowed a thorough classification of all the possible low-symmetry phases and an unambiguous characterization of the phase transitions. Up to our best knowledge this is the first study in which LTPT and DFPT are used together to predict new structural phases of crystals.

Ab initio methods based on DFT are the most powerful theoretical tools for studying structural, electronic and vibrational properties of materials on very realistic grounds. The plane-wave (PW) pseudopotential approach and the local-density approximation (LDA) to DFT have provided a simple framework whose applicability and predictive power have been widely demonstrated. In particular the method has been applied, since the very early years of development, to the study of structural properties of materials, including the relative stability of different phases as determined by the application of an external pressure. A very well known example is shown in Fig. 1.7, where the energy *vs.* volume calculations of Yin and Cohen [15] for Silicon are pictured. These calculations correctly predicted the diamond-to-β-tin transformation at critical pressure within 20% or better of experiment. Also the calculation of reliable phonon spectra is well within the reach of DFT, as it has been shown by Baroni *et al.* within DFPT [16], and very good results have been obtained for pure semiconductors and their superlattices and alloys.

In what follows, we first give a description of the theoretical tools used in this work, LTPT and DFPT, and of the computational techniques necessary to implement them. We then apply this method to predict the equilibrium and lattice-dynamical properties of Cesium halides. Then, a complete description of the phase transitions that occur in

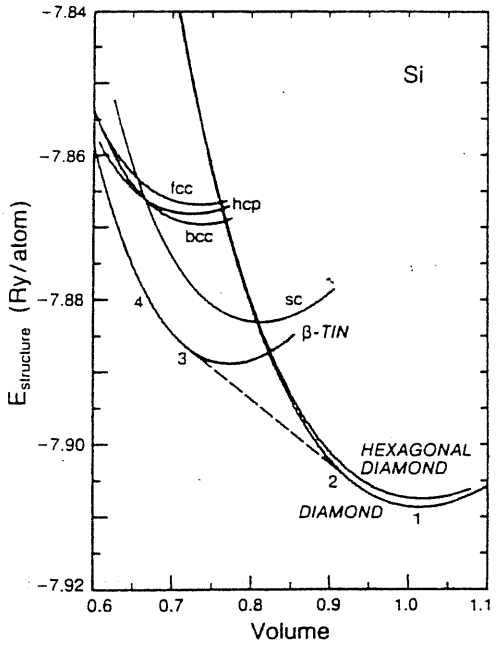

Figure 1.7: Equation of state for Silicon, calculated by Yin and Cohen [15] for seven crystal structures. The slope of the dashed line gives the critical pressure for transformation from diamond to β-tin structure. From Ref. [15].

CsI is given together with results on dynamical and electronic properties at high pressure. Our results confirm our initial conjectures. In fact, the structural phase transition in CsI is shown to be driven by the softening of an acoustic phonon at the M point of the Brillouin zone, which occurs at about 23 GPa. A strong coupling between the soft mode and a tetragonal distortion makes the transition first order, occurring at a slightly lower pressure, and stabilizes the experimentally observed orthorhombic structure with respect to other competing phases. The same analysis is also performed for CsBr and CsCl, and the different behaviours of these compounds is discussed, giving eventually a general picture of the high-pressure phases of all of the Cesium halides. Finally, the high-pressure phases of other alkali halides are also briefly discussed.

2 Theoretical tools

In this chapter we will describe the theoretical framework in which our study has been performed. The key tools are the Landau Theory of Phase Transitions (LTPT) and Density-Functional Perturbation Theory (DFPT).

2.1 Landau Theory of Phase Transitions

In this section we will briefly review the basic results of LTPT that are relevant to our study. For a complete description we refer to Landau's textbook in *Statistical Physics* [18]. Structural phase transitions occur when a material changes its crystallografic structure due to a modification of some external variable, like temperature or pressure. Here we will limit our discussion to those cases where the high-pressure (or low-temperature) phase has a lower symmetry than the low-pressure (or high-temperature) one. Mathematically, this is equivalent to say that the symmetry group of the low-symmetry phase is a subgroup of that of the high-symmetry one. A phase transition can be characterized by certain quantities, called "order parameters", whose expectation value is different from zero in the low-symmetry phase and zero in the high-symmetry one.

In a structural phase transition it is natural to connect the order parameter with the atomic displacements that characterize the low-symmetry phase. Atomic displacements

can be represented as a superposition of the vibrational normal modes of the system, and in this way we can classify them in terms of the normal modes and their symmetry properties. In the simplest case, the order parameter of the phase transition is associated to a single normal mode. When the phonon mode associated to the order parameter is degenerate, the displacement is described by the superposition of the n degenerate normal modes, and n is the number of components of the order parameter (or its dimensionality). In the language of group theory, the displacements of the atoms are functions which transform according to an irreducible representation of the group of the crystal in the undistorted phase. The symmetry properties of such representation give direct informations on the possible stable structures in the less symmetric phase. Moreover, in many structural phase transitions the size and shape of the unit cell alters, and to describe such modifications we must include terms that depend on the infinitesimal strain parameters ϵ as secondary order parameters.

In the Landau theory of structural phase transitions it is *assumed* that the free energy of one unit cell of the system may be expanded in a power series of the order parameter u:

$$\mathcal{F}(V,u) = \mathcal{F}_0 + \alpha u + \frac{1}{2}Au^2 + Du^3 + Bu^4 + ... \tag{2.1}$$

where the coefficients are continuous functions of temperature or pressure and the expansion includes terms up to fourth order for simplicity of discussion. If the states for $u = 0$ and $u \neq 0$ are distinguishable for their symmetry, the first order term must be identically zero, in order to ensure stability to the high-symmetry phase in which $u = 0$. We can classify the different cases according to the values of the parameters in the expansion (2.1). The global stability of eq. (2.1) implies that the quartic term must be positive, and

the local stability of the high symmetry phase is ensured by a positive quadratic coefficient. In this regime, the existence of a stable low-symmetry phase is linked to the value of the coefficient of the cubic term. If $D^2 - 4AB < 0$ the high-symmetry phase is always more stable, while for $D^2 - 4AB > 0$ other stable structures can exist (see Fig. 2.1(a,b)). In this case, the transition from the high- to the low-symmetry phase is discontinuous, and it is said to be of first order. Other stable phases can exist also if the quadratic coefficient is negative (while the stability of the high-symmetry phase is ensured by the quartic coefficient). According to the value of D the transition can be still discontinuous (first order), or continuous. Continuous phase transitions are only possible if $D \equiv 0$ identically. In this case, the second-order coefficient must be zero at the transition, but > 0 in the more symmetric phase and < 0 in the less symmetric one. The transition is then classified as a second-order one (see Fig. 2.1(c)). So far, we have assumed $B > 0$. If B is negative, the stability of the system is ensured by the six-th order terms that must be included in the expansion and whose coefficient must be positive. If for $B < 0$ low-symmetry stable phases exist, the phase transition is always discontinuous, and then of first order.

At all the structural phase transitions the order parameter is coupled to the elastic strains by terms in the free energy which are linear in the strain and quadratic in the order parameter. Then the free energy is generalized to include the strains as:

$$\mathcal{F}(V,u) = \mathcal{F}_0 + \frac{1}{2}Au^2 + Du^3 + Bu^4 + C\epsilon u^2 + \frac{1}{2}c\epsilon^2 ... \tag{2.2}$$

where C is the coupling constant and c is the appropriate elastic constant. Using the condition for the material to be stress-free, $\frac{\partial \mathcal{F}}{\partial \epsilon} = 0$, which gives $\epsilon = -\frac{Cu^2}{c}$ we can eliminate ϵ from eq. (2.2) and we see that the presence of such coupling renormalizes the fourth

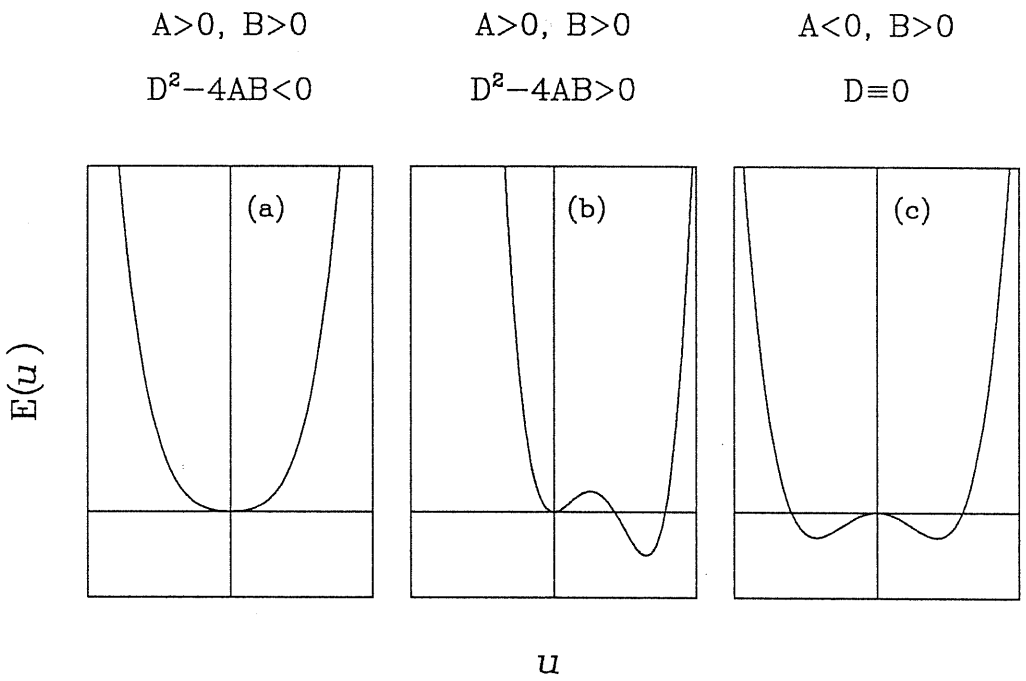

Figure 2.1: Sketch of the behaviour of the free energy (2.1) as a function of the order parameter u. For the discussion of the different cases see the text.

order coefficient as

$$\tilde{B} = B - \frac{C^2}{2c}. \tag{2.3}$$

Eq. (2.3) shows that $\tilde{B}$ is smaller than B (and possibly negative), and consequently, transitions under vanishing stress are more likely to be of first order.

To conclude this short introduction, it is important to notice that there are also cases in which the order parameter of the transition is only the cell shape, *i.e.*, the strain state of the crystal. These are the so-called "martensitic" transitions. It is a general result of group theory that these transitions have first order character, and the formal justification of this assertion for a transition from a cubic to a tetragonal phase is given in section 3.3.

2.2 Density Functional Theory and Lattice Dynamics

The above phenomenological discussion on structural phase transitions was based on the knowledge of the free energy of the system in terms of the atomic displacements. For an application to real systems, it is then necessary a quantitatively detailed description of both the energetics and lattice dynamics of the system on a microscopic basis. Within this work this is attained by means of the Density-Functional Theory (DFT) and its relation to the lattice dynamics.

In the spirit of the Born-Oppenheimer approximation, in the actual calculations the electronic and ionic degrees of freedom are decoupled. Ionic cores behave as classical particles and, given a certain ionic configuration, their potential energy is given by the ground state energy of the electrons which constitute a quantum many-body system. This approach relies on the large mass difference between ions and electrons, which implies that electrons remain very close to their ground state configuration while the ions move. For this reason, the knowledge of the electronic ground state allows a complete description of the properties of the system. DFT provides a theoretical framework to calculate ground state properties of a quantum many-electron system, without solving the many-body Schrödinger equation, which would be an impossible task, due to the large number of degrees of freedom involved in the calculation. A central result of DFT is that the ground state energy of a system of interacting electrons can be obtained—at least in principle—by minimizing the functional [19]:

$$E[n(\mathrm{r})] = F[n(\mathrm{r})] + \int V(\mathrm{r})\, n(\mathrm{r})\, d\mathrm{r}, \tag{2.4}$$

where $F[n]$ is a universal functional of the electronic density (*i.e.* it is independent on $V(\mathrm{r})$), and $V(\mathrm{r})$ is the external potential in which the electrons move, that in crystals

corresponds to the potential generated by the ion cores. The form of $F[n]$ is in general unknown, and in order to apply this theory in actual calculations, Kohn and Sham proposed for this functional the *ansatz*:

$$F[n(\mathbf{r})] = T_0[n(\mathbf{r})] + \frac{1}{2}\int \frac{n(\mathbf{r})\, n(\mathbf{r}')}{|\mathbf{r}-\mathbf{r}'|}\, d\mathbf{r}d\mathbf{r}' + E_{xc}[n(\mathbf{r})]. \tag{2.5}$$

$F[n]$ consists of a Hartree term, corresponding to the classical electromagnetic interaction between the electrons, and a term $T_0[n]$ due to the kinetic energy of a noninteracting electron system with density $n(\mathbf{r})$ (Hartree units are used throughout the discussion). Equation (2.5) defines the exchange and correlation energy $E_{xc}[n]$ as the difference between the unknown functional $F[n]$ and the known terms in its r.h.s.. Minimizing the above functional with the constraint $\int n(\mathbf{r})\, d\mathbf{r} = N$, we obtain a set of self-consistent equations [20]:

$$\left(\hat{H}_{SCF} - \epsilon_i\right)\psi_i(\mathbf{r}) = 0. \tag{2.6}$$

$$\hat{H}_{SCF} = -\frac{\nabla^2}{2} + \underbrace{V(\mathbf{r}) + \int \frac{n(\mathbf{r}')}{|\mathbf{r}-\mathbf{r}'|}\, d\mathbf{r}' + v_{xc}(\mathbf{r})}_{V_{SCF}(\mathbf{r})} \tag{2.7}$$

$$n(\mathbf{r}) = \sum_i \psi_i^*(\mathbf{r})\psi_i(\mathbf{r})\theta(\epsilon_i - \epsilon_F).$$

These are the well known Kohn-Sham equations, where the Fermi energy ϵ_F is defined by the constraint on the number of electrons in the system and $v_{xc}(\mathbf{r}) = \delta E_{xc}[n]/\delta n(\mathbf{r})$ is the exchange-correlation potential. Due to the unknown exchange and correlation potential, the Kohn-Sham equations are of no practical use, unless an approximation for v_{xc} is specified. The most used approximation in practical calculation is the so-called *Local Density Approximation* (LDA). In the LDA, the exchange-correlation energy is taken as a local function of the density itself: $E_{xc}[n] = \int n(\mathbf{r})\, \epsilon_{xc}(n(\mathbf{r}))\, d\mathbf{r}$, where $\epsilon_{xc}(n(\mathbf{r}))$ is

the exchange-correlation energy per particle of the homogeneous electron gas at a density equal to the local density $n(\mathbf{r})$. In this way the potential v_{xc} is given by:

$$v_{xc}(\mathbf{r}) = \mu_{xc}(n(\mathbf{r})) = \frac{\mathrm{d}}{\mathrm{dn}}[n\epsilon_{xc}(n)].$$

From the solution of the Kohn-Sham equations, we get the following expression for the ground-state energy of the system:

$$\begin{aligned} E[\{\psi_i\}, V] &= -\frac{1}{2}\sum_i \theta(\epsilon_i - \epsilon_F) \int \psi_i^*(\mathbf{r})\nabla^2\psi_i(\mathbf{r})\, d\mathbf{r} + \int V(\mathbf{r})n(\mathbf{r})\, d\mathbf{r} + \\ &\quad \frac{1}{2}\int \frac{n(\mathbf{r})n(\mathbf{r}')}{|\mathbf{r}-\mathbf{r}'|}\, d\mathbf{r}d\mathbf{r}' + \int n(\mathbf{r})\epsilon_{xc}(n(\mathbf{r}))\, d\mathbf{r}. \end{aligned} \tag{2.8}$$

Here, $\psi_i(\mathbf{r})$ is the ith wavefunction where the global index $i \equiv (v, \mathbf{k})$ being v the valence band index and $\mathbf{k}$ the wavevector in the first Brillouin zone. From the knowledge of the electron-density distribution we can extract information also on the forces acting on the atoms. Suppose that the external potential depends on a set of parameters $\{\lambda\}$ in the external potential, $V_{\{\lambda\}}(\mathbf{r})$, the Hellman-Feynman theorem [21] states that the derivative of $E_{\{\lambda\}}$ with respect to λ is given by the ground state expectation value of the derivative of the potential with respect to the parameter:

$$\frac{\partial E_{\{\lambda\}}}{\partial \lambda} = \int n_{\{\lambda\}}(\mathbf{r}) \frac{\partial V_{\{\lambda\}}(\mathbf{r})}{\partial \lambda}\, d\mathbf{r}. \tag{2.9}$$

This is a direct recipe to calculate, for instance, forces on atoms, *i.e.* first derivatives of the energy with respect to atomic displacements. Also the stress tensor, *i.e.* derivative of the energy with respect to strain, can be calculated in this way [22]. Differentiating eq. (2.9) with respect to λ', directly yields the second derivative:

$$\frac{\partial^2 E_{\{\lambda\}}}{\partial\lambda\partial\lambda'} = \int \frac{\partial V_{\{\lambda\}}(\mathbf{r})}{\partial\lambda}\frac{\partial n_{\{\lambda\}}(\mathbf{r})}{\partial\lambda'}\, d\mathbf{r} + \int \frac{\partial V(\mathbf{r})}{\partial\lambda\partial\lambda'} n_{\{\lambda\}}(\mathbf{r})\, d\mathbf{r}. \tag{2.10}$$

Suppose now that the $\{\lambda\}$ parameters in (2.10) represent ionic displacements, $u_{\alpha i}(\mathbf{R})$, then the second derivatives of the energy E are simply related to the matrix of the force constants:

$$C_{\alpha i,\beta j}(\mathbf{R}-\mathbf{R}') \equiv \frac{\partial^2 E}{\partial u_{\alpha i}(\mathbf{R})\partial u_{\beta j}(\mathbf{R}')} = C^{ion}_{\alpha i,\beta j}(\mathbf{R}-\mathbf{R}') + C^{elec}_{\alpha i,\beta j}(\mathbf{R}-\mathbf{R}'), \qquad (2.11)$$

The first term in the r.h.s., C^{ion}, is the ionic contribution to the force constants, which is essentially the second derivative of an Ewald sum, and C^{elec} is the electronic contribution, whose expression is:

$$C^{elec}_{\alpha i,\beta j}(\mathbf{R}-\mathbf{R}') = \int \left(\frac{\partial n(\mathbf{r})}{\partial u_{\alpha i}(\mathbf{R})} \frac{\partial V(\mathbf{r})}{\partial u_{\beta j}(\mathbf{R}')} + n(\mathbf{r}) \frac{\partial^2 V(\mathbf{r})}{\partial u_{\alpha i}(\mathbf{R})\partial u_{\beta j}(\mathbf{R}')} \right) d\mathbf{r}. \qquad (2.12)$$

Here, $\mathbf{R}$ indicates the position of the ion i in the unit cell, and α is a polarization index. Due to translational invariance, the force constants defined in eq. (2.11) depend only on the difference $\mathbf{R}-\mathbf{R}'$, and are conveniently calculated in reciprocal space:

$$C_{\alpha i,\beta j}(\mathbf{R}) = \frac{1}{N} \sum_{\mathbf{q}} e^{i\mathbf{q}\mathbf{R}} \tilde{C}_{\alpha i,\beta j}(\mathbf{q}). \qquad (2.13)$$

Then the electronic contribution can be written as:

$$\tilde{C}^{elec}_{\alpha i,\beta j}(\mathbf{q}) = \int \frac{\partial n(\mathbf{r})}{\partial u_{\alpha i}(-\mathbf{q})} \frac{\partial V(\mathbf{r})}{\partial u_{\beta j}(\mathbf{q})} + \delta_{ij} \int n(\mathbf{r}) \frac{\partial^2 V(\mathbf{r})}{\partial u_{\alpha i}(\mathbf{q}=0)\partial u_{\beta j}(\mathbf{q}=0)} d\mathbf{r}. \qquad (2.14)$$

where $\frac{\partial V(\mathbf{r})}{\partial u_{\beta j}(\mathbf{q})}$ is the linear variation of the ionic potential corresponding to a "Bloch" lattice distortion of the form:

$$u_{\beta j}(\mathbf{R}) = u_{\beta j}(\mathbf{q}) e^{i\mathbf{q}\mathbf{R}},$$

and $\frac{\partial n(\mathbf{r})}{\partial u_{\alpha i}(-\mathbf{q})}$ is the corresponding variation of the electron density. The second term in the r.h.s. of (2.14) depends only on the unperturbed density, and then it is of trivial

calculation. Phonon frequencies are then obtained by diagonalization of the dynamical matrix, $\tilde{D}_{\alpha i,\beta j}(\mathbf{q})$, defined as:

$$\tilde{D}_{\alpha i,\beta j}(\mathbf{q}) = \frac{\tilde{C}_{\alpha i,\beta j}(\mathbf{q})}{\sqrt{M_i M_j}}, \tag{2.15}$$

where the M's are ionic masses.

For simplicity of notation, we use from now on a description in terms of finite difference, and omit polarization and atom indices. The electron density response to a Bloch perturbation $\Delta V^{\mathbf{q}}(\mathbf{r})$ is obtained solving iteratively the following system:

$$\Delta n(\mathbf{r}) = 2\mathrm{Re}\sum_i \psi_i^*(\mathbf{r})\Delta\psi_i(\mathbf{r}) \tag{2.16}$$

$$\left(\hat{H}_{SCF} - \epsilon_i\right)|\Delta\psi_i\rangle = -\Delta V^{\mathbf{q}}_{SCF}|\psi_i\rangle + \sum_j |\psi_j\rangle\langle\psi_j|\Delta V^{\mathbf{q}}_{SCF}|\psi_i\rangle. \tag{2.17}$$

$$\Delta V^{\mathbf{q}}_{SCF}(\mathbf{r}) = \Delta V^{\mathbf{q}}(\mathbf{r}) + \sum_i \int \Delta\psi_i^*(\mathbf{r}')\left(\frac{1}{|\mathbf{r}-\mathbf{r}'|} + \frac{\delta^2 E_{xc}}{\delta n(\mathbf{r})\delta n(\mathbf{r}')}\right)\psi_i(\mathbf{r}')\, d\mathbf{r}', \tag{2.18}$$

where $\Delta\psi_i(\mathbf{r})$ are the linear variation of the wavefunctions induced by the perturbation. This system can be solved using standard conjugate-gradient minimization methods, as it is shown in Appendix A. Once the perturbed electron density is known the calculation of dynamical matrices is straightforward, and dynamical properties are calculated with a numerical effort comparable to that of a calculation of unperturbed ground state properties.

In polar crystals, as in the case of Cesium halides, particular care must be taken to compute dynamical matrices at $\mathbf{q} = 0$. In fact, the long-range character of the Coulomb forces gives rise to macroscopic electric fields for LO phonons in the limit $\mathbf{q} \to 0$. Within linear response theory, electric fields can be dealt with exploiting the well known analytic properties of the dynamical matrix. The details of the method that allows the "first-principle" calculation of the lattice dynamical properties of crystals can be found in Ref.

[24], together with the formulas that allow the actual calculations. The derivation of the key equations of DFPT from a variational approach is given in Appendix A.

3 Results

In this chapter we present the results of the calculations of the static and vibrational properties of Cesium halides at different volumes and for different crystal structures. First, we describe some thecnical details of the calculations and discuss the pseudopotential used to describe the ionic cores; we present the results for the static and lattice-dynamical properties of CsI, CsBr, and CsCl, and analyze the properties of these compounds at high pressure. In particular we focus first on CsI, that is the compound most studied and that shows the most interesting behaviour, also in connection to the problem of band-overlap metallization. Later, we generalize our discussion to the other Cesium compounds and finally we study the stability of other alkali halides against tetragonal and/or orthorhombic distortions.

3.1 Computational details

Our calculations are performed in the framework of the LDA plane-wave pseudopotential method. The electron-gas exchange-correlation energy and potential used here, are those determined by Ceperley and Alder [25] as interpolated by Perdew and Zunger [26]. In all calculations the sums over electronic eigenstates in the Brillouin Zone (BZ) have been performed using the 4, 10 or 20 special point mesh for the simple cubic structure in the

Monkhorst and Pack scheme [29]. Plane waves up to a kinetic energy cutoff of 25 Ry were included in the basis set.

We have generated fully non-local pseudopotentials for Cs, I, Br and Cl assuming the following form:

$$V_{\rm ion}(\mathbf{r},\mathbf{r}') = v_{\rm loc}(r)\,\delta(r-r') + \frac{1}{r^2}\sum_l P_l(\widehat{\mathbf{r}\mathbf{r}'})\,\delta(r-r')\,v_l(r), \tag{3.1}$$

where the P_l's are projectors over the l angular momentum states. For Cs and I we have used the pseudopotentials generated with the Kerker's procedure [27] and previously utilized in Ref. [12], where parameters are tabulated. For Br and I, we have generated new pseudopotentials using the method originally proposed by von Barth and Car [28]. The resulting potentials are then fitted to the following analytical form:

$$v_{\rm loc}(r) = \frac{-Z_v}{r}\,\mathrm{erf}(r\sqrt{\alpha_c}), \qquad v_l(r) = (a_l + b_l r^2)\exp(-\alpha_l r^2). \tag{3.2}$$

Ionic pseudopotential parameters generated for Br and Cl, are reported in Table 3.1. Electrons up to Cs $4d$ have been considered as core electrons. The inclusion of the Cs $5s$ and $5p$ states into the valence shell is needed in order to obtain sensible results. In fact we found that pseudopotentials which sustain only the Cs $6s$ electron as a valence electron, yield a monotonic lowering of the energy at decreasing volume, with no stability at all. An explicit account for the non-linear core-correction [30], suggested by the large size of the Cs core, does not substantially improve the situation. The stability of alkali halides is due to the orthogonalization-induced repulsion between neighboring anionic and cationic orbitals. In most applications of the pseudopotential technique to semiconducting and metallic materials, the repulsion exerted by the ionic pseudopotential mainly acts on orbitals centered around the ion itself, which are therefore atomic-like. A much more

Bromine $Z_v = 7, \alpha_c = 1.0418$			
	l=0	l=1	l=2
α_l	1.4214	1.0871	1.0044
a_l	10.3522	4.0326	0.1078
b_l	-6.6640	-2.0113	0.1337
Clorine $Z_v = 7, \alpha_c = 1.7427$			
	l=0	l=1	l=2
α_l	1.7209	1.3181	1.0480
a_l	10.8927	3.4611	-3.1846
b_l	-7.0063	-1.9352	0.8678

Table 3.1: Ionic pseudopotential parameters for Br and Cl.

difficult task is to proper account for the orthogonality effects between off-center orbitals. To cope with the above drawback, we have preferred to include the Cs $5s$ and $5p$ orbitals in the valence shell. In this way the orthogonality between neighboring orbitals is accounted for exactly and the effect of the relaxation of the cationic core, not negligible in such a "large" ion like Cs, are taken into account. Moreover, the inclusion of Cs $5s$ and $5p$ does not affect significantly the numerical labour of the computation. In fact, the spatial extension of these orbitals is comparable to that of the I $5s$ and $5p$ orbitals and then the plane-wave basis set necessary to describe the latter is also adequate for the former.

		a_0	B_0	B_0'
CsI	*theor.*	4.44	15.4	3.84
	expt.	4.56[a]	13.5(2)[a]	5.45(6)[a]
CsBr	*theor.*	4.17	20.7	5.20
	expt.	4.28[b]	17.9[b]	–
CsCl	*theor.*	3.99	24.3	5.84
	expt.	4.12[c]	22.9[d]	–

Table 3.2: Structural parameter fitted to the Murnaghan equation of state for the four compounds studied. Units are Å for a_0 and GPa for B_0. Experimental values are: ([a]) from Ref. [13], ([b]) from Ref.[32], ([c]) from Ref.[33], ([d]) from Ref.[34]. The uncertainty on the last figure in the experimental data is indicated in parenthesis.

3.2 Equilibrium properties of Cesium halides.

We have computed the equation of state of Cesium halides fitting total energies and pressures to the Murnaghan equation of state [31]:

$$P(V) = \frac{B_0}{B_0'}\left(X^{-3B_0'} - 1\right), \qquad X = \left(\frac{V}{V_0}\right)^{1/3}, \tag{3.3}$$

where V_0 is the equilibrium volume, B_0 the bulk modulus, B_0' the first derivative of B_0 with respect to pressure at $V = V_0$. In Table 3.2 the zero-pressure structural properties are compared with available experimental values. The comparison with the experimental data is quite satisfactory. In the following we will use our calculated lattice constants as equilibrium reference values. In Table 3.3 phonon frequencies calculated at high symmetry points Γ and M at the equilibrium volume are compared with experimental data for Cesium halides. The agreement is quite satisfactory and gives us confidence in the predictive power of our calculations.

		$\omega_{TO}(\Gamma)$	$\omega_{LO}(\Gamma)$	$\omega_{TA}(M)$	$\omega_{LA}(M)$	$\omega_{TO}(M)$	$\omega_{LO}(M)$
CsI	*theor.*	2.09	2.85	1.17	1.30	1.48	2.35
	expt.	1.91(5)[a]	2.74(1)[b]	1.29(6)[a]	1.34(5)[a]	–	2.26(5)[a]
CsBr	*theor.*	2.44	3.53	1.27	1.48	1.98	2.79
	expt.	2.29(2)[c]	–	1.22(3)[c]	1.61(3)[c]	1.77(5)[c]	2.69(5)[c]
CsCl	*theor.*	3.33	5.06	1.24	1.86	3.18	4.04
	expt.	3.17(2)[d]	–	1.19(3)[d]	1.90(2)[d]	2.77(2)[d]	3.75(3)[d]

Table 3.3: Comparison between calculated and experimentally observed phonon frequencies of Cesium halides at zero pressure, at the Γ and M points of the BZ. Units are THz. The uncertainty on the last figure in the experimental data is indicated in parenthesis. Experimental data: ([a]) from Ref. [35], ([b]) from Ref. [36], ([c]) from Ref. [37], ([d]) from Ref. [38].

3.3 Properties of CsI at high pressure.

In this section we study the relative stability of various phases of CsI (cubic, tetragonal and the newly proposed orthorhombic structure) at high-pressure. The cubic-to-tetragonal transition reported in Refs. [4, 5] was originally thought to be second-order. Group-theoretical considerations show that this transition must be first-order, and a discontinuity in the order parameter, c/a, at the transition was actually found in both semiempirical [8] and first-principles [9, 12] calculations. As Anderson and Blount have shown [6], transitions from a cubic to a tetragonal structure in which the only order parameter is the unit cell shape cannot be second order. The components of the strain tensor which describe a tetragonal distortion of a cubic cell, $\epsilon_1 = \frac{1}{\sqrt{6}}(2\epsilon_{zz} - \epsilon_{xx} - \epsilon_{yy})$ and $\epsilon_2 = \frac{1}{\sqrt{2}}(\epsilon_{xx} - \epsilon_{yy})$, transform according to the Γ_3^+ irreducible representation of the cubic O_h group. The free

energy of the system can be written as:

$$\mathcal{F} = \mathcal{A} + \frac{1}{2}\mathcal{B}(\epsilon_1^2 + \epsilon_2^2) + \mathcal{C}\sum_{ijk}\epsilon_i\epsilon_j\epsilon_k + \dots \tag{3.4}$$

In order to have a second-order phase transition $\mathcal{C} \equiv 0$ identically, *i.e.* it must be impossible to construct third order invariants with ϵ_1 and ϵ_2. This is not the case, in fact, the unitary representation Γ_1^+ is contained into the cube of the Γ_3^+ irreducible representation, and a third order invariant exist. As shown in Ref. [6] it is given by:

$$\frac{1}{4}(\epsilon_1^2 - 3\epsilon_2^2)\epsilon_1 = [\epsilon_{zz} - (\epsilon_{xx} + \epsilon_{yy})][\epsilon_{yy} - (\epsilon_{zz} + \epsilon_{xx})][\epsilon_{xx} - (\epsilon_{yy} + \epsilon_{zz})], \tag{3.5}$$

Thus the transition is necessarily first order.

Even so, this transition is associated with a dramatic softening of the shear constant, $c_s = \frac{1}{2}(c_{11} - c_{12})$ (the appropriate elastic constant for a tetragonal distortion of a cubic cell) which in fact vanishes at a volume slightly below the transition [8, 12]. The shear constant is also proportional to the square of the sound velocity along the (110) direction for vibrations polarized along $(1\bar{1}0)$. This observation suggests that the softening of the shear constant could induce the softening of a transverse phonon along the (110) direction. In fact, the gliding of one of the (110) planes—which was indicated in [13] as characterizing the low-symmetry phase of CsI—represents a lattice distortion which is very similar to that associated to a doubly degenerate acoustic phonon mode at the M point of the Brillouin Zone (BZ), M_5^-. In Fig. 3.1 we display the ionic displacements along the normal coordinates of the M_5^- acoustic phonon[1]. Note that the displacement pattern is similar to, but different from that proposed in [13] (the magnitude of the cationic and anionic displacements are here different, their ratio depending on the actual dynamical

[1] What we actually mean here by "phonon normal coordinates" are the eigenvectors of the matrix of the interatomic force constants. This definition would coincide with the usual one when the phonon frequency vanishes, or when the atomic masses are equal.

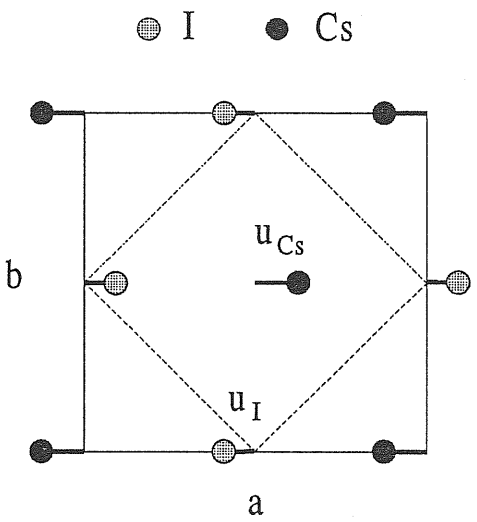

Figure 3.1: Atomic displacements corresponding to an M_5^- acoustic phonon, viewed on the (001) plane. The magnitude of Cesium displacements, $\mathbf{u}_{Cs}$, with respect to Iodine displacements, $\mathbf{u}_I$, is exaggerated for clarity. The solid line indicates the unit cell of the distorted (orthorhombic) structure, while the cell of the undistorted (cubic) structure is indicated by a dashed line. Iodine atoms lie on a plane shifted along the z direction by $\frac{c}{2}$ with respect to the Cesium plane. In the cubic structure one has $a = b = \sqrt{2}c$.

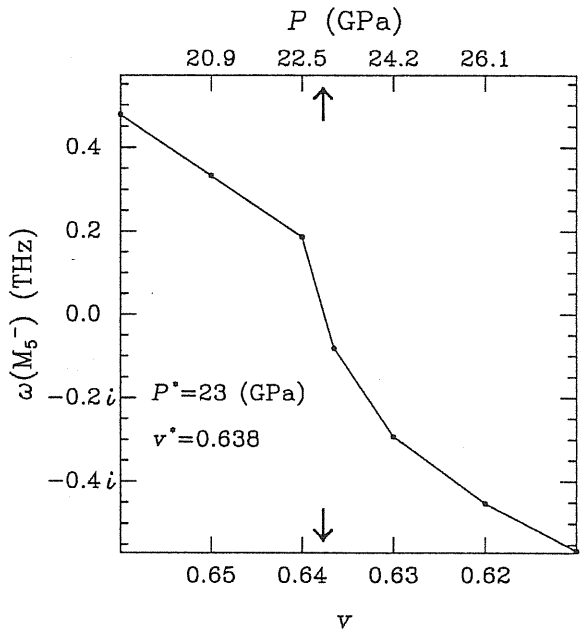

Figure 3.2: Frequency of the M_5^- phonon as a function of molar volume (lower scale, $v \equiv V/V_0$, where V_0 is the equilibrium volume) and of the pressure (upper scale). Arrows indicate the softening volume (v^*) and pressure (P^*).

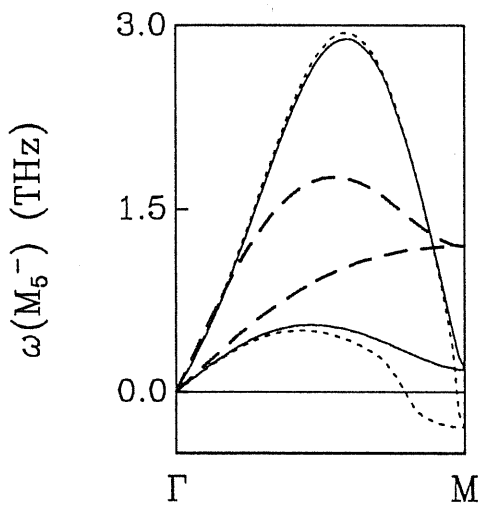

Figure 3.3: Lower portion of the acoustic dispersion along (110) at equilibrium volume (dashed line), and at volumes slightly above (full line - $V/V_0 = 0.63$) and below (point line - $V/V_0 = 0.64$) the mode softening.

matrix of the crystal). In Fig. 3.2 the frequency of the M_5^- phonon as a function of molar volume and of the pressure is shown. The M_5^- phonon softens at $v \equiv V/V_0 = 0.638$, corresponding to a pressure $P \approx 23$ GPa, as a consequence of the incipient softening of the sound velocity of one of the transverse branches, as it is clear in Fig. 3.3, where the acoustic branches of the phonon spectrum for the equilibrium volume and two volumes slightly above and slightly below the mode softening are drawn.

The vanishing of the frequency of the M_5^- mode signals the onset of a phase transition, whose order parameter is the amplitude of the atomic displacements along the phonon normal coordinates. The small group of the M point—whose coordinates are $(\frac{1}{2}\frac{1}{2}0)$—is D_{4h} and its star is made of three equivalent points. The M_5^- mode transforms according to the doubly degenerate Γ_5^- irreducible representation of D_{4h}, so that the order parameter associated with this mode is six-dimensional. According to the Landau theory,[18] the transition can be second order if no third-order cubic invariant can be constructed with the components of the order parameter. This is manifestly the case here, since the Γ_5^-

representation is odd. Assuming that the sixth- and higher-order terms in the expansion of the free energy in powers of the order parameter are positive in the neighborhood of the high-symmetry phase, the transition is then first- or second-order, according to whether the fourth-order invariants are negative or positive, respectively. In our case the free energy of the system coincide with the crystal enthalpy, because the temperature is fixed to zero throughout all the calculations.

In order to write the enthalpy expansion, Eq. (2.1), we must construct all the possible invariants of the phonon-phonon coupling up to the fourth order in the order parameter u, *i.e.* all the invariant combinations of the products $u_i u_j u_k u_l$. Every u_i is a vector in real space whose coordinates measure the amplitude of an atomic displacement corresponding to one of the degenerate M_5^- phonon modes. The displacement depicted in Fig. 3.1 corresponds, for instance, to u_1 in our choice of direct space basis. The procedure to obtain all these invariants is described in detail in Appendix B. Here we give only the result, including also the second order term:

$$\begin{aligned} H_{ph-ph} \;=\; & \mathcal{A}(u_1^2+u_2^2+u_3^2+u_4^2+u_5^2+u_6^2)+\mathcal{A}'(u_1^2+u_2^2+u_3^2+u_4^2+u_5^2+u_6^2)^2+ \\ & \mathcal{B}_1(u_1^4+u_2^4+u_3^4+u_4^4+u_5^4+u_6^4)+\mathcal{B}_2(u_1^2u_2^2+u_3^2u_4^2+u_5^2u_6^2)+ \\ & \mathcal{B}_6[-u_1u_2(u_3^2+u_4^2-u_5^2-u_6^2)+u_3u_4(u_5^2+u_6^2-u_1^2-u_2^2)+ \\ & u_5u_6(u_1^2+u_2^2-u_3^2-u_4^2)]+\mathcal{B}_3(-u_1u_2u_3u_4-u_1u_2u_5u_6+u_3u_4u_5u_6) \quad (3.6) \end{aligned}$$

According to Ref. [39], the possible stable phases occur only along particular directions in the order parameter space *i.e.* to a particular combination of phonon displacements. A classification of the possible phases and their symmetry is given in Appendix B. In our case, the coefficients of the fourth order invariants have been determined in the particular case $V/V_0 = 0.58$, by fitting their values to DFT calculations performed for

$\mathcal{A}$	$\mathcal{A}'$	$\mathcal{B}_1$	$\mathcal{B}_2$	$\mathcal{B}_6$	$\mathcal{B}_3$
-0.00378	0.02011	-0.00621	0.04558	0.04082	-0.17560

Table 3.4: Coefficients of the enthalpy expansion. Units are a.u.

a few lattice distortions. Their values are summarized in Table 3.4. All these invariant turn out to be positive, thus indicating that the transition would be second-order. Group-theoretical considerations considerably restrict the number of possible low-symmetry phases. According to [39], there are seven distorted crystal structures of 'maximal isotropy' (each structure corresponds to a different 'direction' in the six-dimensional configuration space of the order parameter). In the present case, an analysis of the crystal energy reveals that below the transition the only energy minimum occurs along the so called 'P11' direction [39] (which corresponds to the simultaneous excitation of all the six degenerate soft modes). The space group of the low-symmetry phase is T^5, whose tetrahedral symmetry cannot be reconciled with the observed X-ray diffraction patterns [13].

The above considerations hold in the hypothesis that the strain state of the crystal is constant across the transition, except for the isotropic compression due to the application of a hydrostatic pressure. However we know that the softening of the M_5^- phonon mode is closely related to the softening of the shear constant of the crystal, so that a strong coupling between the soft mode and macroscopic strain (i.e. between zone-center and zone-border acoustic phonons) is to be expected. We consider next the expression of the Landau enthalpy of the crystal up to fourth order in the phonon displacements, including the coupling with the strain.

If we include the coupling between phonons and elastic deformation of the cell, the

complete expression of the Landau enthalpy per cell reads:

$$H = H_{ph-ph} + H_{ph-str} + H_{elastic} \tag{3.7}$$

To write the phonon-strain coupling contribution to the enthalpy we have to construct all the possible fourth-order invariants with u and the strain components ϵ . This is done in Appendix B. The result for H_{ph-str} is:

$$\begin{aligned} H_{ph-str} &= C_1\frac{1}{3}(\epsilon_{xx}+\epsilon_{yy}+\epsilon_{zz})(u_1^2+u_2^2+u_3^2+u_4^2+u_5^2+u_6^2)+ \\ & C_2[(2(u_1^2+u_2^2)-u_3^2-u_4^2-u_5^2-u_6^2)(2\epsilon_{zz}-\epsilon_{xx}-\epsilon_{yy})+ \\ & 3(u_3^2+u_4^2-u_5^2-u_6^2)(\epsilon_{xx}-\epsilon_{yy})]+ \\ & C_3(-2u_1u_2-u_3u_4-u_5u_6)(\epsilon_{xx}-\epsilon_{yy})+(-u_3u_4+u_5u_6)(2\epsilon_{zz}-\epsilon_{xx}-\epsilon_{yy})+ \\ & C_4(u_1^2-u_2^2)\epsilon_{xy}+(u_3^2-u_4^2)\epsilon_{yz}+(u_5^2-u_6^2)\epsilon_{xz}. \end{aligned} \tag{3.8}$$

Moreover the elastic energy terms must be included in the enthalpy expansion. For a cubic crystal this reads:

$$\begin{aligned} H_{elastic} &= \frac{1}{2}c_{11}(\epsilon_{xx}^2+\epsilon_{yy}^2+\epsilon_{zz}^2)+c_{12}(\epsilon_{xx}\epsilon_{yy}+\epsilon_{xx}\epsilon_{zz}+\epsilon_{yy}\epsilon_{zz})+ \\ & \frac{1}{2}c_{44}(\epsilon_{xy}^2+\epsilon_{xz}^2+\epsilon_{yz}^2)-P_0\Omega_{cell}(\epsilon_{xx}+\epsilon_{yy}+\epsilon_{zz}) \end{aligned} \tag{3.9}$$

where c_{11}, c_{12} and c_{44} are the three independent elastic constants, and the last linear term takes into account the external pressure for each volume. The values of the coefficients of the phonon-strain coupling and the elastic constant for $V/V_0 = 0.58$ are summarized in Table 3.5. These coefficient have been determined, as the $\mathcal{B}$'s in Eq. (3.6), through DFT calculations performed for different lattice distortions. We find that the 'P11' minimum previously found is unaffected by such a coupling, while four out of the other six maximal isotropy directional minima are slightly modified, still maintaining

$\mathcal{C}_1$	$\mathcal{C}_2$	$\mathcal{C}_3$	$\mathcal{C}_4$	c_{11}	c_{12}	c_{44}
0.00007	0.02570	0.02996	-0.09320	6.524	6.431	6.332

Table 3.5: Coefficients of the enthalpy expansion for the phonon-strain coupling and elastic constants. Units are a.u.

the saddle-point character they would have ignoring the phonon-strain coupling. This coupling changes instead the character of the minima along the other two maximal isotropy directions, 'P1' and 'P2', turning them from saddle points to true minima. The 'P1' structure corresponds to the excitation of just one transverse acoustic phonon (see Fig. 3.1) and it has a much lower energy minimum than that of the 'P2' structure (corresponding to the simultaneous excitation of two degenerate soft phonons at the same point of the BZ), when the coupling with strain is neglected. The observed X-ray diffraction pattern from the low-symmetry phase of CsI [13] is indeed compatible with the space group of the 'P1' structure, D_{2h}^5, which, furthermore, is geometrically simpler than the 'P2' one. For these reasons, in the following we will concentrate on the 'P1' distortion only.

Projecting equation (3.7) along the 'P1' direction, the power expansion of the crystal enthalpy reads:

$$H(u,\epsilon_1,\epsilon_2) = \frac{1}{2}ku^2 + au^4 + \frac{1}{2}c_s\epsilon_1^2 + \frac{1}{2}c_{44}\epsilon_2^2 + (b_1\epsilon_1 + b_2\epsilon_2)u^2 + \mathcal{O}(u^6), \tag{3.10}$$

where $u = u_1$ is the amplitude of the phonon displacement along $(1\bar{1}0)$, $b_1 = \frac{1}{12}\mathcal{C}_1 - 2\mathcal{C}_2$, $b_2 = \mathcal{C}_4$, $\epsilon_1 = \frac{1}{2}(\epsilon_{xx}+\epsilon_{yy}-2\epsilon_{zz})$, and $\epsilon_2 = \epsilon_{xy}$, ϵ_{ij} being the strain tensor. By eliminating ϵ_1 and ϵ_2 from Eq. (3.10) by the equilibrium condition $\partial H/\partial\epsilon_1 = \partial H/\partial\epsilon_2 = 0$, one obtains:

$$\epsilon_1 = -\frac{b_1u^2}{c_s}; \quad \epsilon_2 = -\frac{b_2u^2}{c_{44}}, \tag{3.11}$$

$$\tilde{H}(u) = \frac{1}{2}ku^2 + \left(a - \frac{b_1^2}{2c_s} - \frac{b_2^2}{2c_{44}}\right)u^4 + \mathcal{O}(u^6). \tag{3.12}$$

Eq. (3.12) shows that the coupling between the soft phonon and macroscopic strain renormalizes the fourth-order coefficient, making it large and *negative*, whenever c_s or c_{44} are small enough. Due to the ongoing softening of the shear constant, c_s, we do find that at the softening pressure the fourth-order coefficient is negative, and we conclude that the transition must then be first-order, occurring at a somewhat lower pressure. A thorough study of the transition might be performed by considering the expansion of the crystal energy up to sixth order in the order parameter, and by fitting the relevant coefficients to first-principles calculations, as it was done when the coupling to the strain was neglected. We have preferred instead to perform straight energy minimizations with respect to u and σ along the 'P1' line, in correspondence to different volumes, in such a way to directly obtain the equation of state of the crystal in the low-symmetry phase. The Maxwell construction gives then a transition pressure of ≈ 21 GPa, corresponding to a volume in the cubic phase $V/V_0 \approx 0.64$. In Fig. 3.4 we report the structural parameters of the orthorhombic phase, calculated for different values of the pressure/volume. All the structural parameters, including volume, are discontinuous at the transition pressure as a consequence of its first-order character. The volume discontinuity is very weak (0.1%) and it is not visible on the scale of the figure. Note also the different magnitude of the Cesium and Iodine displacements, and the very weak dependence of b/a upon applied pressure. the different behavior of $c/a - 1$ and $b/a - 1$ with respect to pressure is due to the fact that the former is inversely proportional to the nearly vanishing shear constant, c_s, whereas the latter depends on c_{44} which is regular in this pressure range. In Fig. 3.5 we compare the enthalpy of the new orthorhombic phase (relative to that of the cubic phase)

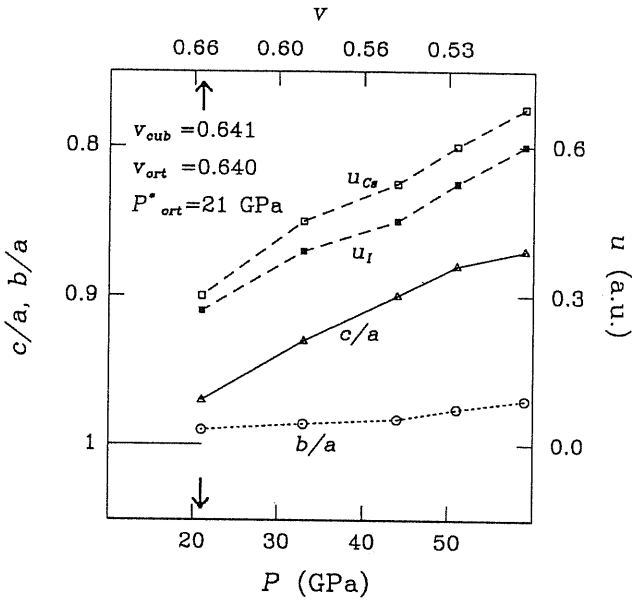

Figure 3.4: Structural parameters of the orthorhombic phase (see Fig. 3.1) of CsI as functions of different values of the volume/pressure. Arrows indicate the transition pressure/volume. The volume discontinuity at the transition is not visible on the scale of the picture. P^*_{ort} indicates the transition pressure, while v_{cub} and v_{ort} are respectively the volumes of the high- and low-symmetry phases at the transition.

with that of the tetragonal phase previously conjectured to occur at higher pressures. The orthorhombic phase turns out to be more stable all over the explored pressure range. In Fig. 3.6 we display our pressure vs. volume data calculated for three different structures (cubic, tetragonal, and orthorhombic) and compare them with the equations of state fitted to experimental data from [7] and [13]. Our data are somewhat intermediate with respect to the previous equations of state, displaying a consistent decrease of the pressure when passing from the cubic to the tetragonal and orthorhombic phases.

In this work we have investigated the band structure of CsI for various volumes in the limits of LDA and restricting our study to the non-relativistic case. Results of our calculations are reported in Fig. 3.7, where it is reported the band structure for three different residual volumes of the cubic cell. The main feature upon squeezing the volume,

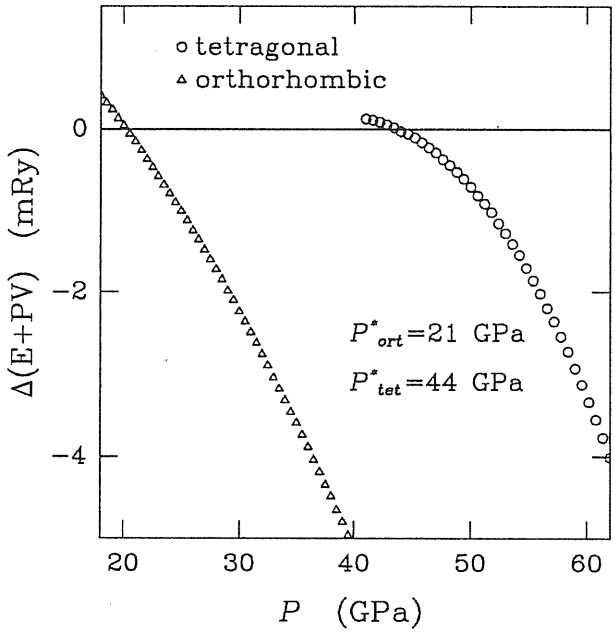

Figure 3.5: Enthalpies of the orthorhombic and tetragonal phases, relative to the enthalpy of the cubic phase, as functions of the applied pressure. P^*_{ort} and P^*_{tet} are the transition pressures from the cubic to the tetragonal and orthorhombic phases respectively.

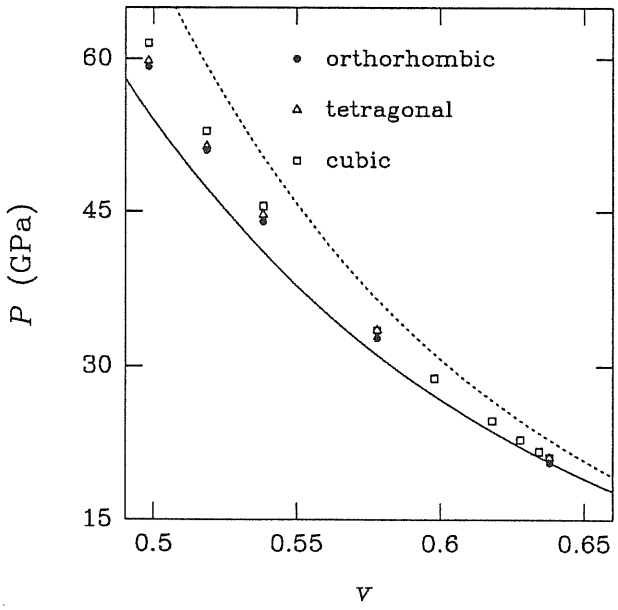

Figure 3.6: Pressure vs. volume data calculated in the present work for different phases of CsI, compared to previous equations of state (dashed line from [7] and continuous line from [13]), fitted to experimental data.

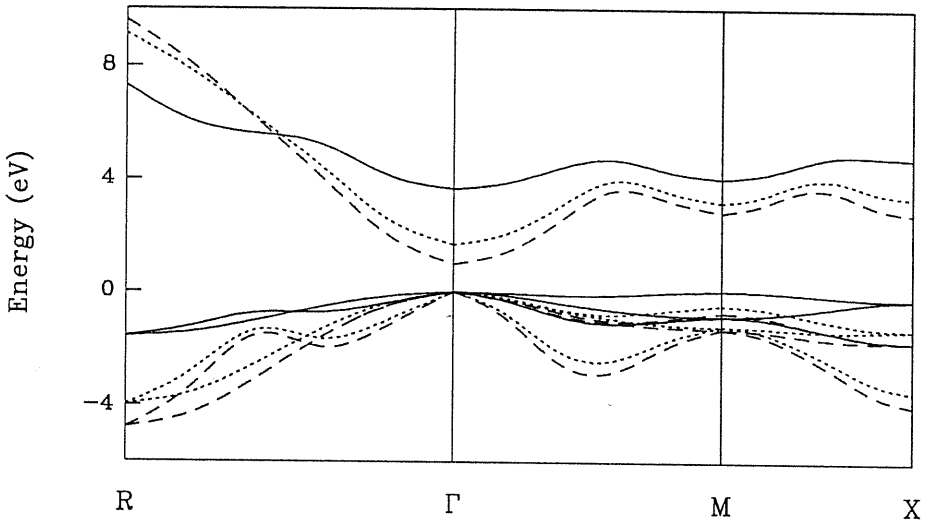

Figure 3.7: Electronic band structure of CsI calculated for three different molar volumes in the cubic phase. The continuous line corresponds to equilibrium volume, while dotted and dashed lines correspond to $V/V_0 = 0.63$ *and* 0.54 *respectively.*

is the gap closure in Γ, responsible for the incoming metallization. We have also studied the effect of the various lattice distortion on the gap, and the results are summarized in Fig. 3.8. For a given molar volume, the tetragonal distortion tends to lower the gap, in agreement with preceding calculations [9], while the orthorhombic one increases it. We find metallization at $V/V_0 = 0.52$, $P = 53$ GPa in the cubic structure, $V/V_0 = 0.54$, $P = 45$ GPa in the tetragonal structure and at $V/V_0 = 0.51$, $P = 55$ GPa in the orthorhombic structure. In the paper by Satpathy *et al.* [9], the enhancement of metallization in the tetragonal and orthorhombic phase was explained in terms of the reduction of the lattice constant in one direction with respect to the cubic case, that affects the electronic states on top of the valence band (TVB), mainly I $5p$, and on the bottom of the conduction band (BCB), mainly Cs and I $5d$, in Γ. The TVB is triply degenerate, has Γ_{15} symmetry

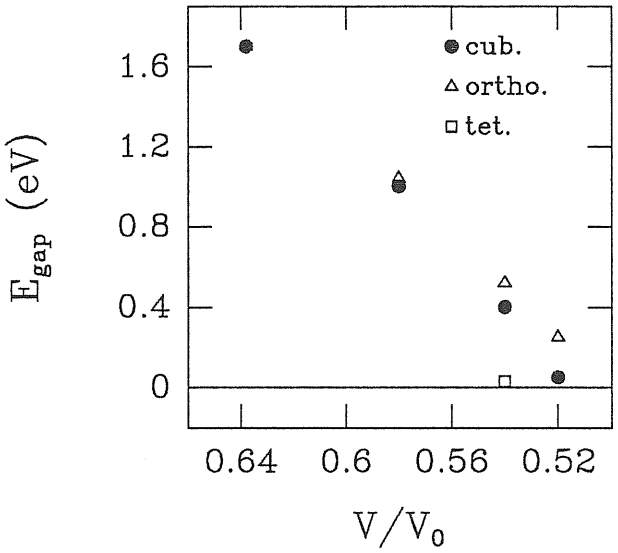

Figure 3.8: Band gap as a function of molar volume for the three different structures.

and consists of antibonding I $5p$ orbitals along x, y and z directions. In the primitive orthorhombic cell the state along the direction of the shortest lattice constant has higher energy than the simple cubic one at the same volume. A similar effect is responsible of the energy lowering of the bonding state $3z^2 - 1$ in the BCB, Γ_{12}. This is no longer true in the orthorhombic D_{2h}^5 structure, where the relative displacements of Cs and I atoms compensate the lowering of the lattice constant in one direction, hence diminishing the tendency of the system to metallization and the strength of interaction between states centered on different atoms. All these results, although they suffer of the well known limitations of the DFT-LDA approach to the electronic properties of crystals, give a qualitative understanding of the electronic implications of the structural phase transitions in CsI.

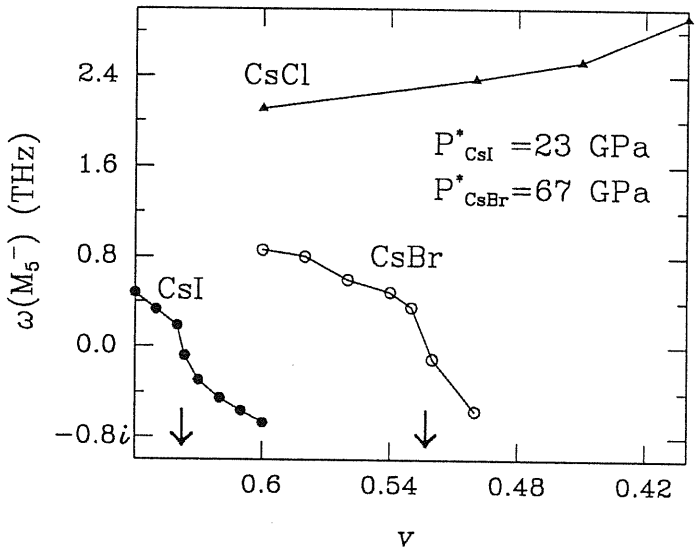

Figure 3.9: Frequency of the M_5^- acoustic phonon as a function of molar volume for CsI, CsBr and CsCl. Arrows indicate the transition volume.

3.4 CsBr, CsCl and other halides

We have also investigated the relative stability of the cubic, tetragonal and orthorhombic phase in CsBr and CsCl. In Fig. 3.9 we display the dependence of the frequency of the M_5^- acoustic phonon upon molar volume in CsI, CsBr and CsCl. As it is clear from the picture, only CsI and CsBr show the softening of the M_5^- acoustic phonon mode upon increasing pressure. A careful study of the two competing phase transitions (cubic-to-orthorhombic and cubic-to-tetragonal) is needed in order to definitely assign the high-pressure phase of CsBr, while for CsCl, the absence of mode softening is a clear indication that the final structure will be tetragonal.

In Table 3.6 we report the molar volume and the pressure corresponding to the two competing phase transitions in Cesium halides. In the first two columns we report the volume and the pressure corresponding to the softening of the zone-boundary phonon in

	cubic-to-orthorhombic *(phonon softening)*		cubic-to-tetragonal	
	v^*	P^*	v^*	P^*
CsI	0.64	23	0.54	45
CsBr	0.52	67	0.54	58
CsCl	–	–	0.54	69

Table 3.6: Molar volume and pressure corresponding to the phonon softening and to the cubic-to-tetragonal transitions in Cesium halides. $v^* = V/V_0$ and P^* is in GPa. The cubic-to-orthorhombic transition in CsI and CsBr occurs at $P^* = 21$ and 66 GPa respectively.

the cubic structure, and the second two the volume and pressure corresponding to the cubic-to-tetragonal transformation.

In CsBr, the tetragonal structure, at variance with the CsI case, turns out to be the most stable all over the explored pressure range, as it is clear in Fig. 3.10, where we compare the enthalpy of the tetragonal and orthorhombic phase relative to the cubic phase. The phonon softening is preceded by the cubic-to-tetragonal transformation, and we have verified that the tetragonal phase is always favoured for all the investigated pressures, and that the phonon-strain coupling induced by the softening of the shear constant does not affect the hierarchy of the transitions. So we can definitely assign the high-pressure phase of CsBr to be tetragonal. The cubic-to-tetragonal transition in CsBr and CsCl has been experimentally observed at 53 ± 2 GPa and 65 ± 5 GPa at the same molar volume $v^* \approx 0.54$ [4]. Our results are in agreement with these measurements.

Finally, we have analyzed the stability of other alkali halides against tetragonal and orthorhombic distortions. The results are summarized in Table 3.7 where the stable phases of various compounds are reported at a residual volume $v = 0.50$. The computational

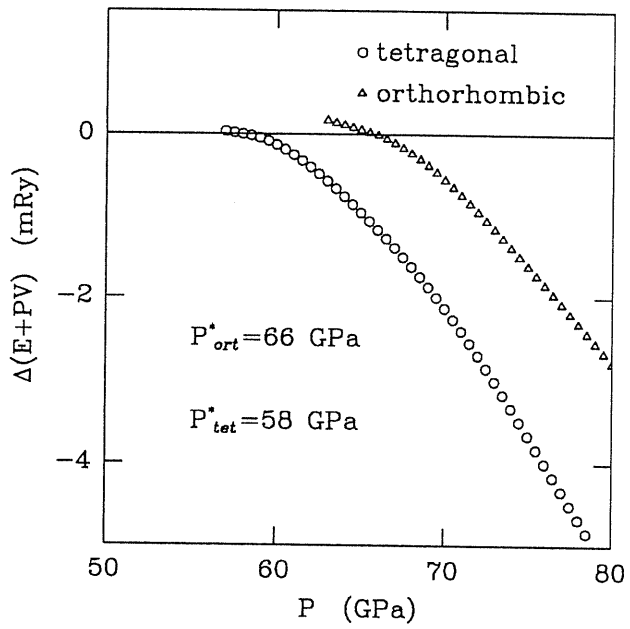

Figure 3.10: Enthalpies of the orthorhombic and tetragonal phases, relative to the enthalpy of the cubic phase, as functions of the applied pressure for CsBr. P^*_{ort} and P^*_{tet} are the transition pressures from the cubic to the tetragonal and orthorhombic phases respectively.

details of these calculations are nearly the same as for the Cesium compounds, although a higher cutoff (35 Ry) is needed in order to get the same degree of convergence. We have generated pseudopotentials for Rb and K with the procedure described in section 3.1. Rubidium and Potassium compounds appear to be stable in the cubic B2 phase all over the explored pressure range and no further distortions of the cell or structural transitions have been observed. These results are in agreement with other calculations performed for Potassium and Sodium compounds [2] in which the cubic B2 phase was reported to be stable up to residual volumes ≈ 0.5 in KCl, while, at our best knowledge, this is the first *ab initio* study of the stability of the high-pressure phase of Rubidium compounds.

	I	Br	Cl
Cs	Ortho. (23) [59]	Tetr. (58) [77]	Tetr. (69) [92]
Rb	Cub. B2 [60]	Cub. B2 [78]	Cub. B2 [99]
K	Cub. B2 [64]	Cub. B2 [92]	Cub. B2 [103]

Table 3.7: Stable phases of various alkali halides at $V/V_0 = 0.5$. For Cesium compounds the pressure at which the compound undergoes a structural transition from the high-pressure cubic B2 phase is indicated in round parenthesis. In square parenthesis the pressure corresponding to $V/V_0 = 0.5$ is reported for every compound. The values are interpolated from the calculated equations of state. Pressures are in GPa.

4 Conclusions

In this work we have analyzed the behaviour of Cesium halides, and in particular of CsI, at very high pressure. The main motivation of the study has been the desire to unify the large variety of theoretical and experimental results present in the literature in a consistent picture, to elucidate the nature of the transitions and to produce a clear classification of the high-pressure phases of Cesium halides. In order to get these results, we have performed extensive Density-Functional Theory calculations of the static and vibrational properties of Cesium halides at high pressure, using the Local Density Approximation, norm-conserving pseudopotentials, and large plane-wave basis sets. All these results have been analyzed in the framework of the Landau theory of phase transitions, that allowed us to classify the different high-pressure phases and the nature of the phase transition.

We focussed our attention mostly on CsI, that is the most studied compound among Cesium halides, and that shows the most original high-pressure behaviour among the members of the family. In fact, as recent experiments have shown, CsI undergoes a structural phase transition from the cubic B2 structure to a more complex orthorhombic phase [13, 14]. We have identified the amplitude of a sixfold degenerate phonon mode (M_5^-) as the relevant order parameter of the transition in the Landau sense. The frequency of

this phonon is found to vanish at a pressure of $\approx$ 23 GPa, which is well below the transition from the cubic to the tetragonal phase. Neglecting the coupling between the soft mode and anisotropic macroscopic strain, we find that the transition would be second-order from the cubic to a tetrahedral (T^5) phase; the coupling with macroscopic strain stabilizes the orthorhombic structure, making the transition first-order, with a very small volume change ($\approx$ 0.1%) and a transition pressure ($\approx$ 21 GPa) slightly below the softening pressure of the M_5^- phonon. We have also found that the orthorhombic structure is always favored with respect to the tetragonal structure, up to pressures of 60 GPa. Furthermore, we have studied the high pressure phases of CsBr and CsCl and we have demonstrated the peculiar character of CsI. In fact, the other Cesium halides undergo a cubic-to-tetragonal transition and, even though in CsBr there is evidence of a phonon softening, the tetragonal phase prevails for all pressures. On the contrary, CsCl does not show any evidence of frequency decrease upon increasing pressure. We have also verified that for Rubidium and Potassium compounds the high-pressure phase is cubic B2 and that such a phase is stable against tetragonal and orthorhombic distortions.

Thus we can conclude that *ab initio* theoretical calculations are able to provide a very reliable picture of the structural properties of Cesium halides. Further work is needed in order to clarify the profound reasons that induce the phonon softening and make the orthorhombic structure energetically favoured at high-pressure only in CsI. There are indications that a key role in the mechanism is played by the empty d orbitals of cation and anion. Calculations done with pseudoatoms in which the d components of the pseudopotentials have been varied "by hand", have shown that in some cases the softening pressure is lowered making the tetragonal structure energetically favoured. However no

final conclusions can be drawn on the basis of such a restricted analysis and a detailed study on this topic is still in progress.

5 Acknowledgements

First of all I would like to thank my supervisor Stefano Baroni for the continuous encouragement and assistance throughout the course of this work. I wish to thank Paolo Giannozzi for the work done together and the kind hospitality he gave me first in Lausanne and then in Pisa. I would like also to acknowledge the fruitful discussions with my friends Stefano De Gironcoli, Marco Bernasconi, and Andrea Dal Corso. I am also happy to thank all the staff of the Scuola Internazionale Superiore di Studi Avanzati for all the technical and administrative assistance they gave me in these four years.

Last but certainly non least, I am particularly grateful to my friend Pasquale Pavone. He taught me his know–how in this field of Solid State Physics and helped me with indispensable suggestions that accompanied the first stages of this work.

Appendix A
Density Functional Perturbation Theory

Density-Functional Linear Response Theory

Here we present a variational formulation of the linear response problem in the framework of DFT. The discussion is based on the method proposed by Baroni *et al.* [16, 24] and we will specialize our variational approach to the case of phonons of arbitrary wavelength.

In order to study the lattice dynamical problem in the linear response approach, we must determine the second order variation of the total energy functional (2.8) with respect to the variation of the wavefunctions and of the perturbing potential.

Let us suppose that a system is disturbed by adding a perturbation $\Delta V(\mathbf{r})$ to the external potential $V(\mathbf{r})$. The Kohn-Sham orbitals will expand accordingly: $\{\psi_i\} \rightarrow \{\psi_i + \Delta\psi_i\}$. Up to the second order in the perturbation the total energy functional reads:

$$\tilde{E}[\{\psi_i + \Delta\psi_i\}, V + \Delta V] = E[\{\psi_i\}, V] + \sum_i \int \frac{\delta E}{\delta \psi_i(\mathbf{r})} \Delta\psi_i(\mathbf{r})\, d\mathbf{r} +$$
$$\int \frac{\delta E}{\delta V(\mathbf{r})} \Delta V(\mathbf{r})\, d\mathbf{r} + \frac{1}{2} \sum_i \int \frac{\delta E^2}{\delta V(\mathbf{r}) \delta \psi_i(\mathbf{r}')} \Delta V(\mathbf{r}) \Delta\psi_i(\mathbf{r}')\, d\mathbf{r} d\mathbf{r}' +$$

$$\frac{1}{2}\sum_{ij}\int \frac{\delta E^2}{\delta\psi_i(\mathbf{r})\delta\psi_j(\mathbf{r}')}\Delta\psi_i(\mathbf{r})\Delta\psi_j(\mathbf{r}')\ d\mathbf{r}d\mathbf{r}'. \tag{A.1}$$

Functional derivatives are as follows:

$$\frac{\delta E}{\delta\psi_i(\mathbf{r})} = 2\hat{H}_{SCF}\psi_i(\mathbf{r}); \qquad \frac{\delta E}{\delta V(\mathbf{r})} = n(\mathbf{r}); \qquad \frac{\delta^2 E}{\delta V(\mathbf{r})\delta\psi_i(\mathbf{r}')} = 2\psi_i(\mathbf{r})\delta(\mathbf{r}-\mathbf{r}');$$

$$\frac{\delta^2 E}{\delta\psi_i(\mathbf{r})}\delta\psi_j(\mathbf{r}') = 2H_{SCF}(\mathbf{r},\mathbf{r}')\delta_{ij} + 2\psi_i(\mathbf{r})\psi_j(\mathbf{r}')\left(\frac{1}{|\mathbf{r}-\mathbf{r}'|} + \frac{\delta^2 E_{xc}}{\delta n(\mathbf{r})\delta n(\mathbf{r}')}\right),$$

where $H(\mathbf{r},\mathbf{r}')$ is the kernel of the operator $\hat{H}$ between states i and j. Rearranging the terms in Eq. (A.1) we write down the second order expansion of the total energy functional as

$$\begin{aligned}
&\tilde{E}[\{\psi_i+\Delta\psi_i\}, V+\Delta V] = \\
&\quad E[\{\psi_i\}, V] + 2\sum_i\int \Delta\psi_i(\mathbf{r})H_{SCF}(\mathbf{r},\mathbf{r}')\psi_i(\mathbf{r})\ d\mathbf{r} + \int n(\mathbf{r})\Delta V(\mathbf{r})\ d\mathbf{r} + \\
&\quad \sum_i\int \Delta\psi_i^*(\mathbf{r})H_{SCF}\Delta\psi_i(\mathbf{r})\ d\mathbf{r} + 2\sum_i\int \psi_i(\mathbf{r})\Delta\psi_i(\mathbf{r})\Delta V(\mathbf{r})\ d\mathbf{r} + \\
&\quad \sum_{ij}\int \Delta\psi_i^*(\mathbf{r})\Delta\psi_j^*(\mathbf{r}')K(\mathbf{r},\mathbf{r}')\psi_i(\mathbf{r})\psi_j(\mathbf{r}')\ d\mathbf{r}d\mathbf{r}',
\end{aligned} \tag{A.2}$$

where

$$K(\mathbf{r},\mathbf{r}') = \frac{1}{|\mathbf{r}-\mathbf{r}'|} + \frac{\delta^2 E_{xc}}{\delta n(\mathbf{r})\delta n(\mathbf{r}')}.$$

This functional must be minimized with the constraint

$$\langle\psi_i+\Delta\psi_i|\psi_j+\Delta\psi_j\rangle = \delta_{ij}.$$

We have then to solve the variational problem:

$$\delta\left(E - \sum_{ij}\lambda_{ij}\left[\langle\Delta\psi_i|\psi_j\rangle + \langle\psi_i|\Delta\psi_j\rangle + \langle\Delta\psi_i|\Delta\psi_j\rangle\right]\right) = 0. \tag{A.3}$$

where λ's are Lagrange multipliers. The variation of Eq. (A.3) with respect to $\Delta\psi_i$ gives:

$$\hat{H}_{SCF}\psi_i(\mathbf{r}) + \hat{H}_{SCF}\Delta\psi_i(\mathbf{r}) + \Delta V_{SCF}(\mathbf{r})\psi_i(\mathbf{r}) - \sum_j\lambda_{ij}(\psi_j(\mathbf{r})+\Delta\psi_j) = 0 \tag{A.4}$$

where

$$\Delta V_{SCF}(\mathbf{r}) = \Delta V(\mathbf{r}) + \sum_i \int \Delta\psi_i^*(\mathbf{r}')K(\mathbf{r},\mathbf{r}')\psi_i(\mathbf{r}')\, d\mathbf{r}'. \tag{A.5}$$

Rearanging the terms in (A.4) we end up with the final system.

$$H_{SCF}\Delta\psi_i(\mathbf{r}) - \sum_j \lambda_{ij}\Delta\psi_i(\mathbf{r}) = -\Delta V_{SCF}(\mathbf{r})\psi_i(\mathbf{r}) + \sum_j (\lambda_{ij} - \epsilon_i\delta_{ij})\,\psi_i(\mathbf{r}). \tag{A.6}$$

A solution of this system would give in principle the answer to the linear response problem. However the direct solution reveals to be an enormous task, du to the large number of variables involved: number of Fourier components of $\Delta\psi$ times the number of states. We can decompose this large system into a restricted number of independent systems (one for each state). To do so let's consider the variation of Eq. (A.3) with respect to λ_{ij}.It gives the equation for the constraints:

$$\langle\Delta\psi_i|\psi_j\rangle + \langle\psi_i|\Delta\psi_j\rangle + \langle\Delta\psi_i|\Delta\psi_j\rangle = 0$$

that is

$$\langle\Delta\psi_i|\psi_j\rangle = \mathcal{O}(\Delta V^2). \tag{A.7}$$

If we multiply Eq. (A.3) by $\langle\psi_l|$ we get

$$\epsilon_l\langle\psi_l|\Delta\psi_i\rangle - \sum_j \lambda_{ij}\langle\psi_l|\Delta\psi_j\rangle = -\langle\psi_l|\Delta V_{SCF}|\psi_i\rangle + \lambda_{li} - \epsilon_i\delta_{li} \tag{A.8}$$

Given the condition (A.7), substituting into Eq. (A.6), retaining only the linear terms, we end up with the linear system:

$$(H_{SCF} - \epsilon_i)\,|\Delta\psi_i\rangle = -\Delta V_{SCF}|\psi_i\rangle + \sum_j |\psi_j\rangle\langle\psi_j|\Delta V_{SCF}|\psi_i\rangle. \tag{A.9}$$

If we consider a given periodic perturbation of wavevector $\mathbf{q}$, $\Delta V^{\mathbf{q}}(\mathbf{r})$, and impose translational symmetry, we can identify the quantities that enters this formulation as

$\psi_i(\mathbf{r}) \equiv \psi_{v,\mathbf{k}}(\mathbf{r})$, $\Delta\psi_i(\mathbf{r}) \equiv \Delta\psi_{v,\mathbf{k}+\mathbf{q}}(\mathbf{r})$, $\Delta V_{SCF}(\mathbf{r}) \equiv \Delta V^{\mathbf{q}}_{SCF}(\mathbf{r})$. In particular, it is important to stress that $\Delta V^{\mathbf{q}}_{SCF}$ when acting on a wavefunction of wavevector $\mathbf{k}$, transforms it into a function of wavevector $\mathbf{k}+\mathbf{q}$, and it should be remarked that the linear response to a perturbation of given $\mathbf{q}$ only contains Fourier components of wavevector $\mathbf{q}+\mathbf{G}$; different $\mathbf{q}$'s do not mix at this order of perturbation theory. Rearranging the terms in (A.9) and recognizing that $\sum_v |\psi_{v,\mathbf{k}}\rangle\langle\psi_{v,\mathbf{k}}| = P_v$ where P_v is the projector over the valence–state manifold, and $P_c = 1 - P_v$ we end up with the final result

$$\left[\epsilon_{v,\mathbf{k}} - H_{SCF}\right] |\Delta\psi_{v,\mathbf{k}+\mathbf{q}}\rangle = P_c \Delta V^{\mathbf{q}}_{SCF} |\psi_{v,\mathbf{k}}\rangle. \tag{A.10}$$

The total first order variation of the density induced by the perturbing potential can be written as

$$\Delta n(\mathbf{r}) = 2\mathrm{Re} \sum_{\mathbf{k}} \sum_{v} \psi^*_{v,\mathbf{k}}(\mathbf{r}) \Delta\psi_{v,\mathbf{k}+\mathbf{q}}(\mathbf{r}) \tag{A.11}$$

Equations (A.5) (A.11) and (A.10) constitute a self–consistent set of equations that can be solved iteratively. The linear system (A.10) has an infinite number of solutions because the determinant of $[\epsilon_{v,\mathbf{k}} - H_{SCF}]$ vanishes, and the vector on the l.h.s. is orthogonal to the null space of $[\epsilon_{v,\mathbf{k}} - H_{SCF}]$. In practice, $\Delta\psi_{v,\mathbf{k}+\mathbf{q}}$ is defined within a multiple of $\psi_{v,\mathbf{k}}$. However such an indeterminacy does not affect the final result because we are interested only in its projection onto the conduction-state manifold. Depending on the size of the basis set, Eq. (A.10) can be solved either by factorization techniques,[40] or by iterative methods. The variational formulation of the DFPT problem can improve the solution of the linear system giving explicit variational formulas for the coefficients of the response functions, and allowing a replacement of the traditional solution methods by a conjugate–gradient algorithm [41], where self–consistency steps are done simultaneously. The method described in this section applies to a general perturbation. The matrix elements necessary

when the perturbation describes a lattice distortion are discussed in Ref. [24] where detailed formulas are explicitly given.

Conjugate–Gradient algorithm.

In this section we will describe the steps that allow the solution of the linear system (A.9) by a conjugate–gradient algorithm. To this aim, let's recast the system in the form:

$$\sum_j \int A_{ij}(\mathbf{r},\mathbf{r}')\Delta\psi_j(\mathbf{r}')\ d\mathbf{r}' = b_i(\mathbf{r}), \tag{A.12}$$

identifying the operator A_{ij} in the l.h.s., and the r.h.s. b_i. To proceed to this identification we can rewrite

$$\Delta V_{SCF}(\mathbf{r}) = \Delta V(\mathbf{r}) + 2\sum_l \int \Delta\psi_i^*(\mathbf{r}')K(\mathbf{r},\mathbf{r}')\psi_i(\mathbf{r}')\ d\mathbf{r}' \tag{A.13}$$

and define

$$\Delta\tilde{V}_{SCF}(\mathbf{r}) = 2\sum_l \int \Delta\psi_i^*(\mathbf{r}')K(\mathbf{r},\mathbf{r}')\psi_i(\mathbf{r}')\ d\mathbf{r}' \tag{A.14}$$

and then

$$\Delta\tilde{V}_{SCF}(\mathbf{r})\psi_i(\mathbf{r}) = 2\sum_l \int \Delta\psi_i^*(\mathbf{r}')K(\mathbf{r},\mathbf{r}')\psi_i(\mathbf{r}')\psi_i(\mathbf{r})\ d\mathbf{r}'. \tag{A.15}$$

Knowing that, we can write

$$\begin{aligned}\sum_l |\psi_l\rangle\langle\psi_l|\Delta\tilde{V}_{SCF}|\psi_i\rangle &= \sum_l \int \psi_l^*(\mathbf{r}'')\Delta\tilde{V}_{SCF}\psi_i(\mathbf{r}'')\psi_l(\mathbf{r})\ d\mathbf{r}'' = \\ &2\sum_{jl}\int\int \Delta\psi_j^*(\mathbf{r}')K(\mathbf{r},\mathbf{r}')\psi_j(\mathbf{r}')\psi_l^*(\mathbf{r}'')\psi_i(\mathbf{r}'')\psi_l(\mathbf{r})\ d\mathbf{r}'d\mathbf{r}'' = \\ &\sum_j \int \left(\sum_l \int \psi_j(\mathbf{r}')\psi_i^*(\mathbf{r}'')\psi_l(\mathbf{r}'')\psi_l(\mathbf{r})K(\mathbf{r},\mathbf{r}')\ d\mathbf{r}''\right)\Delta\psi_j^*(\mathbf{r}')\ d\mathbf{r}'\end{aligned} \tag{A.16}$$

and then we can identify

$$\begin{aligned} A_{ij}(\mathbf{r},\mathbf{r}') &= \begin{cases} H_{SCF}(\mathbf{r},\mathbf{r}') - \epsilon_i\delta(\mathbf{r}-\mathbf{r}'); & \text{if } i=j \\ \psi_i(\mathbf{r}'')\psi_j(\mathbf{r})K(\mathbf{r},\mathbf{r}')+ \\ \quad \sum_l \int \psi_j(\mathbf{r}')\psi_i^*(\mathbf{r}'')\psi_l(\mathbf{r}'')\psi_l(\mathbf{r})K(\mathbf{r},\mathbf{r}')\ d\mathbf{r}'' & \text{otherwise} \end{cases} \\ b_i(\mathbf{r}) &= -\Delta V(\mathbf{r})\psi_i(\mathbf{r}). \end{aligned} \tag{A.17}$$

To perform the conjugate – gradient minimization is then sufficient to compute

$$\sum_j \int A_{ij}(\mathbf{r},\mathbf{r}')\Delta\psi_j(\mathbf{r}')\ d\mathbf{r}',$$

that, once $\Delta\tilde{V}_{SCF}(\mathbf{r})$ is known, is given by:

$$\sum_j \int A_{ij}(\mathbf{r},\mathbf{r}')\Delta\psi_j(\mathbf{r}')\ d\mathbf{r}' = [H_{SCF} - \epsilon_i]\,|\Delta\psi_i\rangle + P_c\Delta\tilde{V}_{SCF}|\psi_i\rangle. \tag{A.18}$$

At this point we have a system that can be solved by a standard conjugate–gradient algorithm. For more details on the minimization procedure see for instance Ref. [42] and references therein.

Appendix B
Symmetry invariants of the Landau Theory

In this appendix we give explicit formulas for the fourth-order invariant polinomials that enter the phonon-phonon and the phonon-strain contributions.

Invariants of the phonon-phonon coupling

The invariant polynomials in u up to the fourth degree can be obtained using standard techniques of group theory [43]. The number of fourth order invariants is equal to four, because the identical representation is contained four times in the 4-th symmetric power of the irreducible representation Γ_5^- of D_{4h}. A way to obtain them is to operate on the possible fourth power combinations of u's with all symmetry operations of the point group O_h of the more symmetric phase. The starting combination must obey some symmetry conditions in order to preserve translational invariance: given $u_i u_j u_k u_l$, $\mathbf{k}_i + \mathbf{k}_j + \mathbf{k}_l + \mathbf{k}_k = \mathbf{G}$, where $\mathbf{k}_i$ is the wave vector for phonon u_i , and $\mathbf{G}$ is a reciprocal space vector. This implies that the two phonons associated to the same $\mathbf{k}$ vector of the star must be always coupled, *i.e.* products if the kind $u_1^3 u_2$ are forbidden. The basic invariants are summarized in Table B.1.

Starting combination	Invariant
$u_1u_1u_1u_1$	$u_1^4+u_2^4+u_3^4+u_4^4+u_5^4+u_6^4$
$u_1u_1u_2u_2$	$u_1^2u_2^2+u_3^2u_4^2+u_5^2u_6^2$
$u_1u_2u_3u_3$	$-u_1u_2(u_3^2+u_4^2-u_5^2-u_6^2)+$
	$u_3u_4(u_5^2+u_6^2-u_1^2-u_2^2)+$
	$u_5u_6(u_1^2+u_2^2-u_3^2-u_4^2)$
$u_1u_2u_3u_4$	$-u_1u_2u_3u_4-u_1u_2u_5u_6+u_3u_4u_5u_6$

Table B.1: Basic invariant polynomials in u up to degree four which enter the free energy expansion Eq. (2.1).

Given the free energy expansion it is possible to find the possible stable phases after the transition along the lines of standard group theory [43]. For our specific case, we refer to Ref. [39], where a complete description of the six-dimensional order parameter case is carried out. Following the notation of Ref. [39], the possible stable phases can be classified as in Table B.2 where each configuration corresponds to a particular direction in the order parameter space, *i.e.* to a particular combination of phonon displacements. We have verified that for each direction there was an energy minimum and for each case we determined the corresponding length of the displacement.

Invariants of the phonon-strain coupling

Consider the generic expression of the Landau free energy projected along a certain direction of the order parameter space:

$$\mathcal{F}=-\omega^2u^2+Iu^4+F[u,\epsilon]$$

where u^n stands for all possible invariant combinations of degree n, and $F[u,\epsilon]$ is the term of phonon - strain coupling, containing all possible products (up to the fourth order) of

	Direction	Symmetry group
P1	(a, 0,0, 0,0, 0)	D_{2h}^5
P2	(a,-a,0, 0,0, 0)	D_{2h}^{19}
P6	(a, 0,a, 0,a, 0)	C_{3v}^5
P7	(0,-a,0, a,0, a)	D_3^7
P9	(a,-a,a,-a,0, 0)	D_{4h}^{17}
P10	(a,-a,0, 0,a,-a)	D_{4h}^{17}
P11	(a,-a,a, a,a, a)	T^5

Table B.2: Classification of the possible stable phases along particular direction of the order parameter space.

the kind:

$$\epsilon^2,\ u\epsilon,\ u^2\epsilon,\ u\epsilon^2,\ u\epsilon^3,\ u^2\epsilon^2,\ u^3\epsilon.$$

All products containing an odd power of u are not invariant and so they cancel. The only remaining products are ϵ^2, that is the elastic energy term, $u^2\epsilon$ and $u^2\epsilon^2$. Up to fourth order only $u^2\epsilon$ must be considered; in fact we can easily demonstrate that $\epsilon \propto u^2$ and so $u^2\epsilon^2$ is actually of sixth order in the order parameter. To see this, we start from

$$\mathcal{F} = -\omega^2 u^2 + I u^4 + \Lambda\epsilon^2 + \alpha u^2\epsilon + \beta u^2\epsilon^2$$

and from the equilibrium condition $\frac{\partial \mathcal{F}}{\partial \epsilon} = 0$ to get

$$2\Lambda\epsilon + \alpha u^2 + 2\beta u^2\epsilon = 0$$

and so

$$\epsilon = \frac{1}{2}\frac{\alpha u^2}{\Lambda + \beta u^2} \propto u^2 + \mathcal{O}(u^4).$$

Q.E.D.

To find the form of the $u^2\epsilon$ invariant we have determined all second order products such that $\mathbf{k}_i + \mathbf{k}_j = \mathbf{G}$. These correspond to a 9-dimensional representation that can

	irrep	Basis functions
3-D	Γ_2	$-u_1u_2 + u_3u_4 + u_5u_6$
	Γ_3	$-2u_1u_2 - u_3u_4 - u_5u_6$; $u_3u_4 - u_5u_6$
6-D	Γ_1	$u_1^2 + u_2^2 + u_3^2 + u_4^2 + u_5^2 + u_6^2$
	Γ_3	$2(u_1^2 + u_2^2) - u_3^2 - u_4^2 - u_5^2 - u_6^2$; $u_3^2 + u_4^2 - u_5^2 - u_6^2$
	Γ_5	$u_1^2 - u_2^2$; $u_3^2 - u_4^2$; $u_5^2 - u_6^2$

Table B.3: Basis functions for the different irreducible representations of the order parameter.

irrep	Basis functions
Γ_1	$\epsilon_{xx} + \epsilon_{yy} + \epsilon_{yy}$
Γ_3	$\epsilon_{xx} - \epsilon_{yy}$; $2\epsilon_{zz} - \epsilon_{xx} - \epsilon_{yy}$
Γ_5	ϵ_{xy}; ϵ_{xz}; ϵ_{yz}

Table B.4: Basis functions for the different irreducible representations of the strain tensor.

be decomposed into a 3-dimensional one: u_1u_2, u_3u_4, u_5u_6, plus a 6-dimensional one: u_1^2, u_2^2, u_3^2, u_4^2, u_5^2, u_6^2. These can be decomposed as: $\Gamma_2 + \Gamma_3$ and $\Gamma_1 + \Gamma_3 + \Gamma_5$ respectively. Knowing that, we constructed the combinations of u's that correspond to the basis functions of the irreducible representations, tabulated in Table B.3

The strain tensor in the group O_h transforms like $\Gamma_1 + \Gamma_3 + \Gamma_5$, and the basis functions that can be constructed are summarized in Table B.4.

The invariant that can be constructed from these basis functions are four (the identical representation is contained four times in the direct products of the representations of the

$u_i u_j \otimes \epsilon$), and they can be obtained as:

$$\phi^{\Gamma_i} = \sum_{\lambda} \epsilon_{\lambda}^{\Gamma_i} (u \otimes u)_{\lambda}^{\Gamma_i}$$

where λ is the index of the basis functions.

Bibliography

[1] H.K. Mao and P.M. Bell, Science **200**, 1145 (1978).

[2] S. Froyen and M.L. Cohen, J. Phys. C **19**, 2623 (1986).

[3] E. Madelung, Phys. Z. **19**, 524 (1918); P.O. Ewald, Ann. Phys. (Leipzig) 64, 253 (1921).

[4] T.-L. Huang and A. Ruoff, Phys. Rev. B **29**, 1112 (1984); T.-L. Huang, K.E. Brister, and A.L. Ruoff, Phys. Rev. B **30**, 2968 (1984); Y.K. Vohra, K.E. Brister, S.T. Weir, S.J. Duclos, and A.L. Ruoff, Science **231**, 1136 (1986).

[5] E. Knittle and R. Jeanloz, Science **223**, 53 (1984); E. Knittle and R. Jeanloz, J. Phys. Chem. Solids 46, 1179 (1985); E. Knittle, A. Rudy and R. Jeanloz, Phys. Rev. B **31**, 588 (1985).

[6] P.W. Anderson and E.I. Blount, Phys. Rev. Lett. 14, 217 (1965).

[7] K. Asaumi, Phys. Rev. B **29**, 1118 (1984).

[8] Y.K. Vohra, S.J. Duclos and A. Ruoff, Phys. Rev. Lett. 54, 570 (1985).

[9] N.E. Christensen and S. Satpathy, Phys. Rev. Lett. **55**, 600 (1985); S. Satpathy, N.E. Christensen and O. Jepsen, Phys. Rev. B **32**, 6793 (1985).

[10] R. Reichlin, M. Ross, S. Martin and K.A. Goettel, Phys. Rev. Lett. **56**, 2858 (1986); Q. Williams and R. Jeanloz, Phys. Rev. Lett. **56**, 163 (1986).

[11] Y.K. Vohra, S.T. Weir, K.E. Brister, A.L. Ruoff, Phys. Rev. Lett. **55**, 977 (1984).

[12] S. Baroni and P. Giannozzi, Phys. Rev. B **35**, 765 (1987).

[13] H.K. Mao, Y. Wu, R.J. Hemley, L.C. Chen, J.F. Shu, and L.W. Finger, Science **246**, 649 (1989); H.K. Mao, Y. Wu, R.J. Hemley, L.C. Chen, J.F. Shu, L.W. Finger, and D.E. Cox, Phys. Rev. Lett. **64**, 1749 (1990).

[14] I.V. Aleksandrov, A.F. Goncharov, I.N. Makarenko, and S.M. Stisov, Phys. Rev. B **43**, 6194 (1991).

[15] M.T. Yin and M.L. Cohen, Phys. Rev. B **26**, 5668 (1982).

[16] S. Baroni, P. Giannozzi, and A. Testa, Phys. Rev. Lett. **58**, 1861 (1987).

[17] M. Buongiorno Nardelli, S. Baroni and P. Giannozzi, Phys. Rev. Lett. **69**, 1069 (1992).

[18] L.D. Landau and E.M. Lifshitz, *Statistical Physics*, Part I (Pergamon, Oxford, 1980), Chap. XIV.

[19] P. Hohemberg and W. Kohn, Phys. Rev. **136**, B864 (1964).

[20] W. Kohn and J.L. Sham, Phys. Rev. **140**, A1133 (1965).

[21] H. Hellmann, *Einführung in die Quantumchemie* (Deuticke, Leipzig, 1937); R.P. Feynmann, Phys. Rev. **56**, 340 (1939).

[22] O.H. Nielsen and R.M. Martin, Phys. Rev. Lett. **50**, 697 (1983).

[23] X. Gonze and J.P. Vigneron, Phys. Rev. B **39**, 13120 (1989).

[24] P. Giannozzi, S. de Gironcoli, P. Pavone, and S. Baroni, Phys. Rev. B **43**, 7231 (1990).

[25] D.M. Ceperley and B.J. Alder, Phys. Rev. Lett. **45**, 566 (1980).

[26] J. Perdew and A. Zunger, Phys. Rev. B **23**, 5048 (1981).

[27] G.P. Kerker, J. Phys. C **13**, L189 (1980).

[28] von Barth and R. Car unpublished.

[29] for a review see for instance W.E. Pickett, Computer Phys. Rep. **9**, 115 (1989)

[30] S.G, Louie, S. Froyen and M.L. Cohen, Phys. Rev. B **26**, 1738 (1982).

[31] F.D. Murnaghan, *Deformation of an elastic solid*, chap. 4, (John Wiley, NY, (1951)).

[32] K. Reinitz, Phys. Rev. **123**, 1615 (1961).

[33] R.W.G. Wyckoff, *Crystal Structures*, (R.E. Krieger Publishing Company, Malabar, 1982), Chap. III.

[34] R.K. Singh, H.N. Gupta and M.K. Agrawal, Phys. Rev. B **17**, 894 (1978).

[35] W.Bührer and W. Hälg, Phys. Status Solidi **46**, 679 (1971).

[36] R.P. Lowndes, Phys. Rev. B **1**, 2754 (1970).

[37] S. Rolandson and G. Raunio, Phys. Rev. B **4**, 4617 (1971).

[38] A.A.Z. Ahmad, H.G. Smith, N. Wakabayashi and M.K. Wilkinson, Phys. Rev. B **6**, 3956 (1972).

[39] J.S. Kim, D.M. Hatch, and H.T. Stokes, Phys. Rev. B **33**, 1774 (1986).

[40] If factorization techniques are used, the best choice is to tridiagonalize first H_{SCF}, and solve then the system in the basis where it is tridiagonal. The advantage is that this allows to perform just one factorization for *all* the systems corresponding to different values of $\epsilon_{v,\mathbf{k}}$.

[41] X. Gonze, D.C. Allan and M.P. Teter, Phys. Rev. Lett. **68**, 3603 (1992).

[42] W.H. Press (et al.), *Numerical Recipies: the art of scientific computing* (Cambridge Univ. Press, Cambridge, 1986).

[43] J.C. Tolédano and P. Tolédano, *The Landau Theory of Phase Transitions*, (World. Sci., Singapore, 1987); M.V. Jarić, Phys. Rev. Lett. **48**, 1641 (1982); D.M. Hatch and H.T. Stokes, *Isotropy Subgroups of the 230 crystallographic Space Groups*, (World. Sci., Singapore, 1988).